# Nano-fibrous scaffold with curcumin for anti-scar wound healing

## 3.1 Introduction

Skin is the vital component of the human body which covers the entire external surface. It constitutes about 8% of the total body mass and forms a unique self-repairing interface between the external environment and the body. Additionally, it forms the first line of body defence and is capable of adsorbing and excreting certain chemical substances, while simultaneously withstanding stretch, compression, and friction [1]. It protects the internal tissues of the body from biological, chemical and physical damages, prevents dehydration and controls water balance in the body. The disruption and disfiguring of the anatomical structure of the skin due to injury has attracted the attention of researchers for developing better dressing materials for prompt healing [2]. Skin wounds are a major healthcare problem causing an increasing number of trauma and pathophysiological conditions.

The process of healing and nature of wounds depends on its site and confinement up to the various layers of skin. Healing of wounds confined to the epidermal layer is quick and takes place through the regeneration of epithelial cells. Full-thickness wounds (FTW) are difficult to heal due to loss of both epidermis and dermis layers resulting in lack of residual cells for regeneration except at the periphery and often leaves scar [3]. Split-thickness skin grafts were used for promoting initial wound healing, but these require a cumbersome and expensive surgery and tend to contract with the passage of time [4]. To get over these issues, tissue-engineered scaffolds mimicking the extracellular matrix (ECM) with various active agents have been used for accelerated healing [5].

The wound healing takes place through three sequential overlapping stages of variable duration, namely hemostasis and inflammatory phase, proliferative phase and tissue remodelling phase. With the loss of skin integrity at the injury site, hemostasis begins and causes release of numerous chemical mediators, pro-inflammatory cytokines, proteolytic enzymes, growth factors and reactive oxygen species (ROS) [5]. The ROS are important for body's natural defence and are responsible for the action of phagocytic cells [6]. Normally, the harmony of ROS is maintained by endogenous anti-oxidant enzymes, such as catalase, superoxide dismutase (SOD) and glutathione peroxidase [7]. In the condition of severe trauma like fatal traumatic wound, burn, and microbial infections, the shortage of oxygen in the injured tissues is responsible for increased inflammatory response. The excess ROS produced under such cases cause harm to the surrounding cellular environment and the fibroblasts cells which are responsible for collagen secretion for the formation of ECM and healing. The elevated level of ROS also causes oxidative stress at the acute wound site and stimulates a cascade of biochemical reactions resulting in delayed healing [8]. Apart from the oxidative stress, other factors like tissue dystrophy, moisture imbalance, infection, trauma, or burns are the other factors affecting epithelialization and granulation processes resulting in delayed wound healing. Thus causing formation of scar at the wound site, one of the critical concerns for cosmetologists and dermatologists [9].

Under natural pathophysiological conditions, the normal wound healing process gets severely deregulated. The large trauma wounds due to severe accidents or burns result in a major loss of skin tissue and thus fail to heal. Such traumatic conditions hamper the typical healing pattern of the skin tissue and become a major a social and financial burden for decades. In such cases, the healing process gets obstructed at the

very initial phase and gradually turns to be chronic due to failure in the healing and may result in tissue necrosis [10]. Therefore, clinical interventions are vital for healing such wounds. Traditional dressings such as bandages, gauzes and cotton wool offer protection against bacteria, but often suffer from limitation of adhesion of the dressing to the wound, causing pain, discomfort and scar when removed. Out of the available strategies, the most successful is to provide an artificial matrix in the form of a wound dressing or skin graft and serve as a provisional matrix and thereby aid in the healing process. Several smart wound dressings or skin substitutes have been developed by numerous researchers to mimic the healing wound or skin microenvironment through cutting edge technologies [4]. The natural wound milieu consists of ECM platform having cell adhesive sites, instructive biochemical cues, growth factors and various types of cells. Mimicking the whole microenvironment is very challenging, and therefore tissue engineers primarily focuses on the structural framework which is of prime importance in healing [5]. On the overall, the wound dressing platform or skin graft assists in rapid healing of the wounds. Furthermore, any specific stage or event of the healing process can be stimulated by certain regulator biomolecules like cytokines, growth factors, chemokines and cell adhesive peptides depending on the type of functionalisation of the matrix [11].

So for better wound care an ideal dressing material would be a biomimetic fibrous scaffold with a diameter in the range of 50-500 nm to match the ECM physical structure that could also support as skeletal material for cell growth for accelerated healing [12]. It must also have a high surface area to volume ratio for promoting hemostasis and surface functionalisation. It should be highly porous (60-90%) for cell respiration, gas permeation and preventing wound dehydration. There should be

interconnected nano-porosity for the prevention of microbial infiltration and cell in-growth. Apart from these, it must also have desired mechanical strength, permit the release of bioactive anti-oxidants and biosorption at the wound site for accelerated healing, and prevent cell rupture and discomfort during removal through its biodegradation [10].

Amongst the various available techniques for developing fibrous mesh like drawing, force-spinning, melt blowing, phase separation, self-assembly, template melt extrusion, template synthesis etc., electrospinning is the method of choice for designing the biomimetic dressing material because of its simplicity, cost-effectiveness and versatility [12,13]. The electrospun dressing material possesses all the properties which are essential for an ideal dressing material. It works under ambient conditions and uses a single-step process which can be scaled up with great diversity of natural and synthetic polymers depending upon the need [5,10,14].

Polyvinyl pyrrolidone (PVP) has been widely used as the base material for biomedical applications as it is non-toxic, soluble in water and many other organic solvents, soft, can retain moisture without losing mechanical integrity, has good film-forming capacity, ability to form inter-polymer complexes with both hydrophobic and hydrophilic substances [2,11,15].

The trivalent cerium ($Ce^{3+}$) salts have been used in the biomedical fields due to their bactericidal, antitumor and anti-oxidant activity [7]. Cerium nitrate has been used in burn wound healing since 1976 [16]. It denatures the lipid-protein complex by binding on the burnt skin and helps to reduce immunosuppression in topical cutaneous burns along with its antimicrobial action [17]. The existence of cerium in a reversible dual oxidation state of $Ce^{3+}$ and $Ce^{4+}$ is responsible for its anti-oxidant enzyme-mimetic

activity. The ROS-scavenging abilities of cerium at the wounded site provides an alternative for protecting the native tissues by enhancing the level of collagen and hydroxyproline for effective wound healing [8].

Curcumin, the yellow-orange polyphenolic compound derived from *Curcuma longa's* rhizome possesses a wide range of therapeutic properties. It has been extensively used in biomedical applications due to its anti-inflammatory, anti-oxidant and anticancer activities [18,19]. The application of curcumin is limited by its low water solubility, high clearance rate and instability at high pH, high temperature and bright light. A variety of routes to maximise the curcumin's bioavailability in the biological system have been adopted. A wide range of encapsulating carriers like microgels, proteins, surfactants and biopolymers have been utilised [20,21].

In the present study, an effort has been made to develop an anti-oxidant loaded composite wound dressing material which could provide a skeletal framework for the granulation tissues in FTW to accelerate the healing activity by tissue regeneration. The biological anti-oxidant curcumin and cerium have been used to protect the injured tissues from ROS and harnessing their medicinal values in wound care management. The biodegradability of the electrospun fibrous scaffold would protect the newly formed tissues from being ruptured as the dressing scaffold would get dissolved with the granulation of tissues. The central hypothesis of this research is that cerium and curcumin loaded nanofibrous scaffold will be associated with decrease in inflammatory oxidative stress and may help in rapid scar free wound healing. It is thought that cerium and curcumin blended nanofibers can protect cells and tissues through their ability to scavenge ROS and promote cell survival under conditions of oxidative stress. It is likely that these nanoparticles also exhibit toxic effects if cellular exposure is excessive. The

observations made and results obtained through these studies are discussed in this chapter.

## 3.2 Literature review

### 3.2.1 Wound care

With an estimated global market of $20.4 billion by 2021, the skin wound dressings are a crucial segment of the wound-care products industry. During the last two decades, this field has seen many advancements since newly designed dressings are considered as materials with the biologic properties required for healing the wounds in the least possible time. The wound dressing materials currently available in the market are typically in the form of foams, films, hydrogels, and sponges [22]. Nanofibrous dressings have emerged as new class of wound dressing materials that offer distinct advantages. Nanofibrous meshes comprising many non-woven intermingled nanofibers provide a large exposed surface area with nanoporosity, that facilitates interaction with the living cells at the wound bed as skeletal framework through the mimicking ECM [5]. It is essential to choose a correct composite material for wound dressing applications. An ideal dressing must possess biocompatibility, biodegradability, minimal cytotoxicity, hemocompatibility, and carry various functional groups to gain multiple biologic and healing properties. They can also carry multiple bioactive compounds with different healing and antimicrobial characteristics [19]. Before going to the details of dressing's basic understanding of the structure and function of skin and different types of wounds with their healing mechanism would be helpful in understanding the role of wound dressings. To understand the roles of different parameters that influence the healing process is also important.

### 3.2.2 Skin

Skin is the largest organ that accounts for approximately 8% of total body mass in adults covering nearly $2\,m^2$ of the body surface area[23]. It enables vital body function to take place in a controlled physiological environment by acting as the barrier between the body and outer environment and regulates a variety of essential protective functions [19].

#### 3.2.2.1 Layers of skin

Anatomically the skin is arranged in three layers: (1) the epidermis, which is an external, non-vascularized epithelium up to 600 μm thick, (2) the dermis, which is composed of connective tissues with a mixture of fibroblasts and is of 2–4 mm in thickness, and (3) the sub-cutis or hypodermis, which is comprised of fatty connective tissues that provide the dermal-skeletal attachment [24,25]. The detailed structure of skin is shown in *Figure* 3.1.

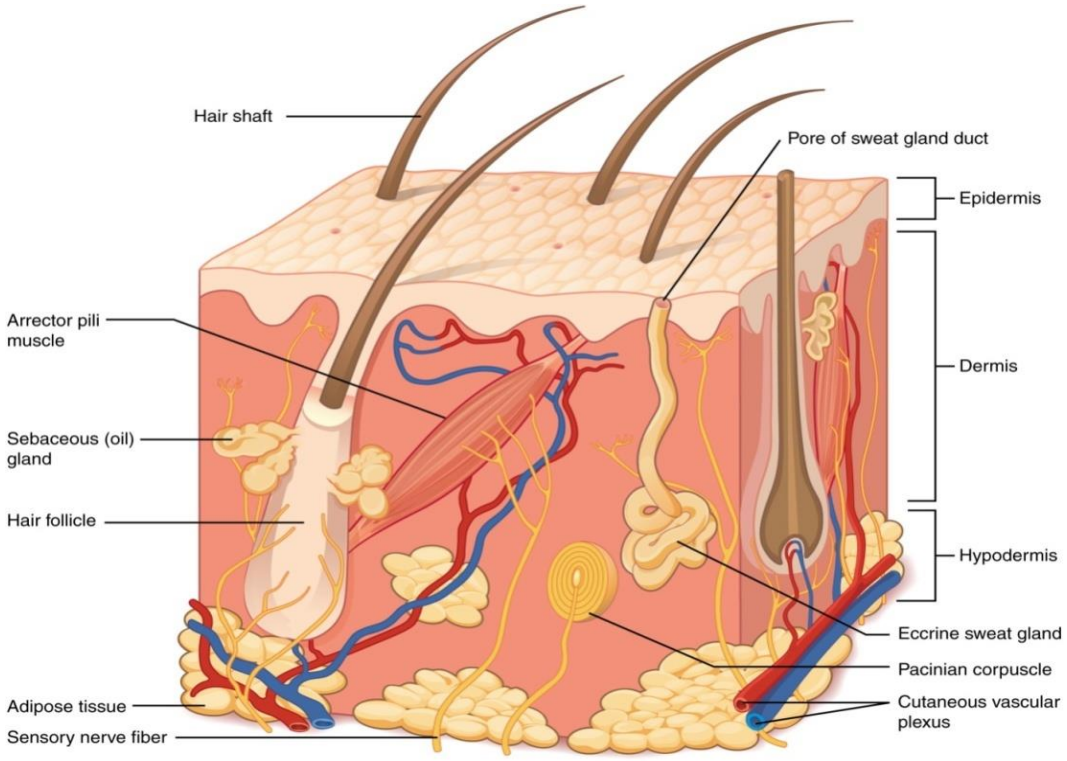


**Figure 3.1:** Layers of skin (Source: Anatomy and Physiology, openstax)

As a protective physical barrier, the skin is constantly exposed to the external environment causing dehydration, chemical and mechanical damage, and microbial infection [26]. The skin pigment absorbs harmful ultraviolet radiation and the immuno-regulatory system constantly scans the microenvironment [24]. When the integrity of the skin is compromised by injuries, the body initiates a multi-step and dynamic process at the injured site, leading to partial healing of the tissue and restoration of the skin's barrier functions. The immediate goal in wound repair is to achieve tissue integrity and homeostasis [27]. Therefore, survival of all mammals depends to a great extent on a robust wound healing process [25].

### 3.2.3 Wound

The loss of protective function of skin due to severe disease or trauma (physical, chemical, thermal or microbial) is known as a wound [28]. This can range from a simple break in the epithelial integrity of the skin or it can be deeper, extending upto the subcutaneous tissue with damage to other structures such as tendons, muscles, vessels, nerves, parenchymal organs and even bone [29]. Irrespective of the cause, a wound damages the tissue and upsets the local environment within it.

The open skin wounds due to a cut, burn, diseases or surgical interventions are commonly observed in our daily life. Such wounds are prone to contamination by different pathogens found in the surrounding environment, endogenous microbes living in the mucous membranes, or by the microflora available on the adjacent skin surface. Bacteria, like *E. coli*, *P. aeruginosa* and *S. aureus* are some of the predominant pathogens responsible for skin contamination and subsequent infections [30].

#### 3.2.3.1 Types of wounds

Wounds can be categorized into acute and chronic wounds depending on the healing time.

##### 3.2.3.1.1 Acute wound

Acute wounds heal normally, as a result of a regulated, predictable and ordered repair process. Sudden loss of anatomical structure owing to surgery or trauma results into acute wounds [31].

##### 3.2.3.1.2 Chronic wound

Chronic wounds fail to proceed through this tightly controlled process and do not recover the previous integrity within three-month period, and remain in a stagnated phase of pathological inflammation [32]. Inflammation and oxidative damages are the

main causes of non-healing chronic wounds as reported through clinical and preclinical studies [6]. Other reason for prolonged healing is the development of drug-resistant bacterial biofilms, persistent infections, failure of epidermal or dermal cells to respond to reparative stimuli, tissue hypoxia, and failed re-epithelialization caused by repeated trauma.

### 3.2.3.2 Types of clinical wound healing

Based on the abrasion, laceration, amount of skin and tissue loss, clinically a wound healing can be accomplished by one of the following ways:

#### 3.2.3.2.1 Primary intention wound healing process

A wound heals by the primary process when it is aseptic and freshly created with minimum tissue loss, and its edges are in close proximity, smooth bordered and surgically closed by a suture (*Figure* 3.2a). Primary wound healing e.g. after a surgical incision, generally occurs within 6-8 days without any complication, and with scanty granulation tissues at the incised gap [33,34].

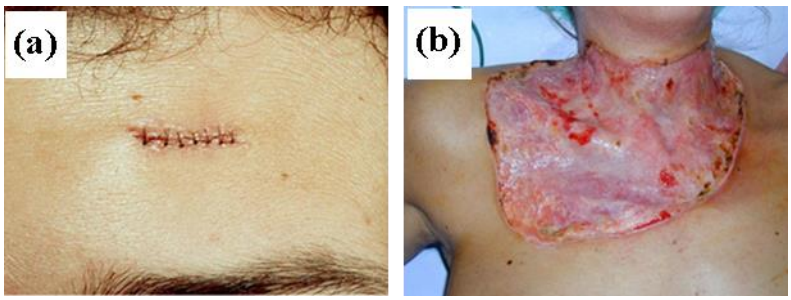


**Figure 3.2:** Clinical wound healing **(a)** Primary intention wound healing process, and **(b)** Secondary intention wound healing process

*Source: https://gmch.gov.in/e-study/e%20lectures/Pathology/L10%20wound%20healing.pdf*

#### 3.2.3.2.2 Secondary intention wound healing process

Secondary healing is a process that uses contraction and epithelialization to restore the epithelial barrier. It takes longer repair time with scar formation. Secondary healing occurs when the wound has lost a considerable amount of tissues and its edges are so distant that it cannot be sutured (*Figure* 3.2b). Wounds are left open and gaps are filled by exuberant granulation tissue deposition and epithelial cell migration. Secondary healing occurs either in acute wound with significant tissue loss or in chronic wounds [28,33].

#### 3.2.3.2.3 Tertiary intention wound healing process

A tertiary intention wound healing is also known as delayed closure. It involves the principles of both primary and secondary healings. It occurs when healing needs to be delayed intentionally, for example when blood perfusion is low or wound is highly infected [33].

### 3.2.4 Wound healing mechanism

The wound healing is a natural recovery response to tissue injury that commences with trauma and ends with the restoration of tissue or body function. Healing is a complex physiological, dynamic, interactive process that involves the participation of various components such as extracellular matrix, soluble mediators, blood and parenchymal cells [35]. The natural process of wound healing comprises four overlapping but well-defined phases: coagulation/hemostasis, inflammation, proliferation and remodelling [23]. These four healing phases involve interactions between various types of cells, bioactive factors and a supporting platform, which is usually the natural ECM secreted by cells. The cascade of wound healing begins with

hemostasis and inflammation. Different phase of healing are shown in *Figure* 3.3 and inherent biological processes are summarized in Table 3.1.

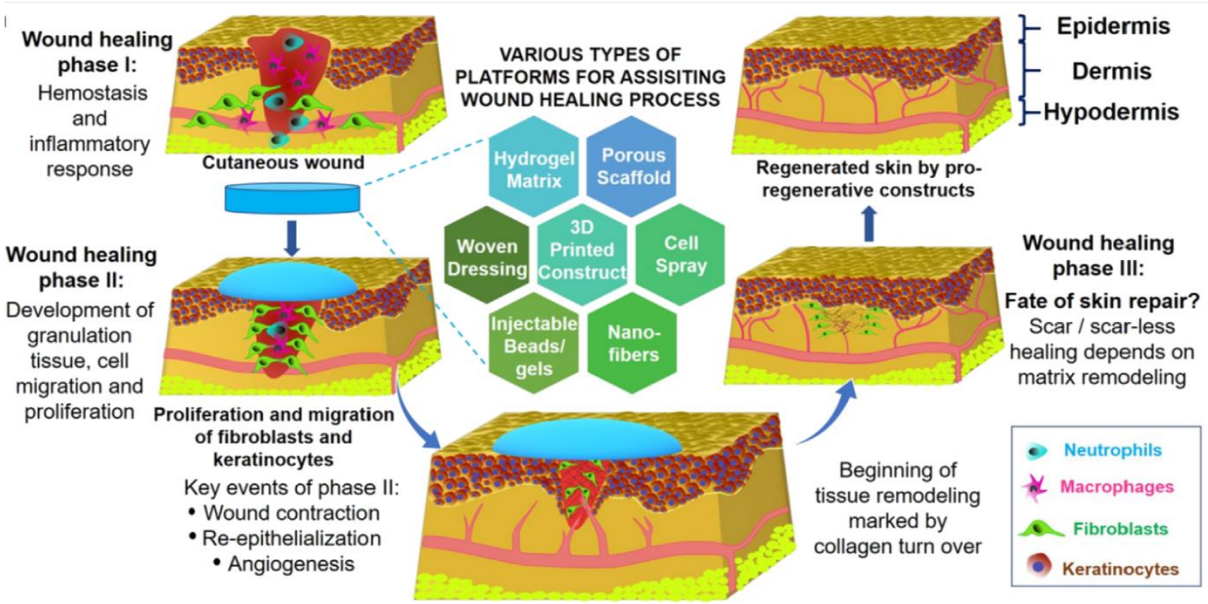


**Figure 3.3:** Schematic representation of the concept of wound healing process assisted by a dressing material or skin graft [36]

**Table 3.1:** Four phases of healing of a full-thickness wound [19,28,33,37]

| Phase | Cellular and bio-physiological changes |
|---|---|
| **Hemostasis phase** | Blood vessels constrict and clotting factors are activated. Clot formation blocks the bleeding and acts as a barrier to prevent bacterial contamination. Platelets release growth factors, which alert various cells to start the repair process at the wound location. |
| **Inflammatory phase** | Vasodilation, chemotaxis activation of inflammatory cells:<br>- Neutrophil infiltration: begin digestion of invading microbes and nonviable tissue<br>- Monocyte infiltration and differentiation to macrophages, principle phagocytic cells, which also releases numerous cytokines for activation of fibroblast, angiogenesis and keratinocytes<br>- Lymphocytes infiltration helps in tissue repair |
| **Proliferative phase** | Four important processes occur in this phase:<br>- Re-epithelialization: new epidermis and granulation tissue are developed<br>- Angiogenesis: New capillaries formation occurs to bring oxygen and nutrients to the wound<br>- Collagen deposition and Native ECM formation: this provides strength and integrity to the wound<br>- Wound Contraction: the wound begins to reduce in size |
| **Maturation (remodelling) phase** | Collagen continues to strengthen the wound, and the wound becomes a scar.<br>Vascular maturation and regression. |

### 3.2.4.1 Hemostasis

Hemostasis occurs upon injury, which constitutes platelet aggregation and thereby blood clot formation [37]. The blood clot is mainly composed of fibrin, fibronectin and activated platelets. Growth factors such as platelet-derived growth factor

(PDGF), transforming growth factors-β (TGF-β) and epidermal growth factor (EGF) recruit fibroblasts, macrophages and neutrophils to the wound site. The blood clot provides a provisional ECM for cell migration [36].

#### 3.2.4.2 The inflammatory phase

The inflammatory phase involves the migration of blood cells, such as phagocytic neutrophils and macrophages, to the wound site [37]. The phagocytes initially remove foreign particles and other ECM debris, while also releasing cytokines to promote fibroblast migration and proliferation towards the end of the inflammatory phase [38].

#### 3.2.4.3 Proliferative phase

The proliferative phase is described by epithelialization, angiogenesis, collagen deposition and granulation tissue formation, and wound contraction. Re-epithelialization of wounds begins within hours of injury [25]. This phase is characterized by the formation of new blood vessels (angiogenesis or neovascularization), which re-establish perfusion to sustain the new tissues [39] and the synthesis and deposition of fragments of ECM proteins such as collagen fibers and granulation tissue characterised by a higher content of Type III collagen [37]. Fibroblasts produce the new ECM necessary to support cell ingrowth using collagen as the building blocks and thus play a crucial role in the wound healing process [38].

#### 3.2.4.4 Maturation or remodeling phase

During the final remodelling stage, angiogenesis is completed, keratinocyte progression effectively seals the wound, and the ECM components organise themselves in a structure resembling that of healthy tissue. A scar tissue is formed, where Type III collagen is re-synthesised as thicker, better organised bundles and levels decrease

similar to unwounded skin [38]. *Figure* 3.4 illustrates the time span of acute wound healing phase following injury and the overlapping nature of the process.

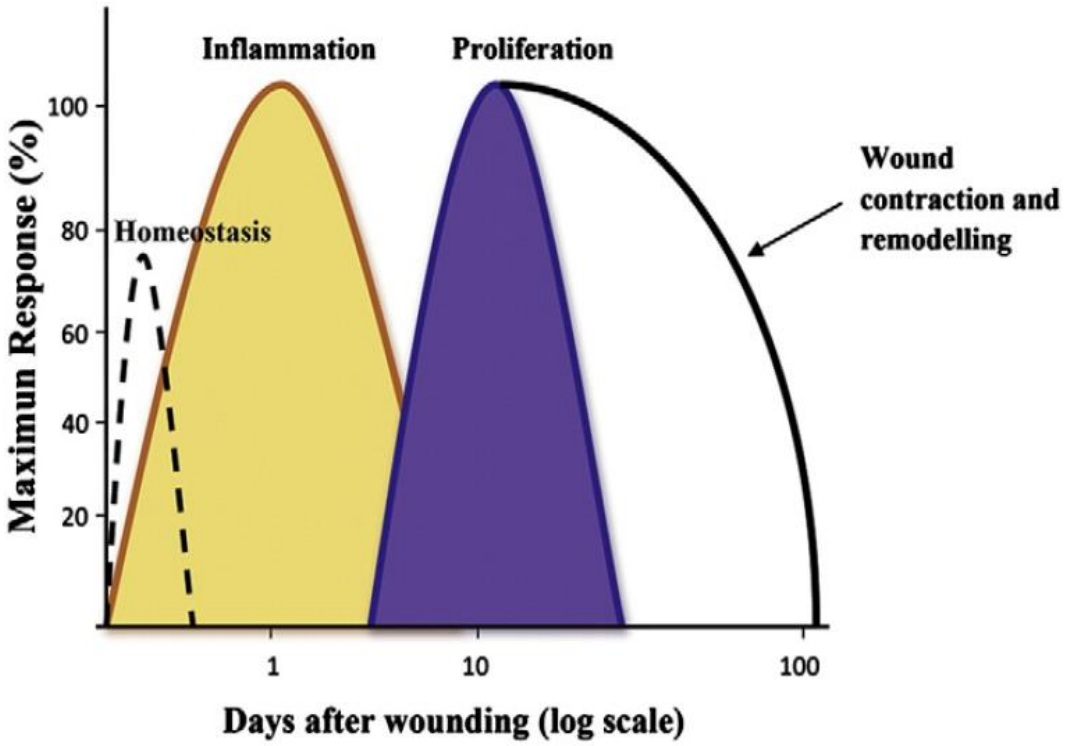


**Figure 3.4**: Four phases of acute wound healing [19]

### 3.2.5 Wound dressings

Dressing is one of the important wound management materials. Wound dressing is defined as a sterile compressed fibrous layer acting as a barrier to protect the injured epidermal tissues from environmental threats and microbial penetration whilst simultaneously promoting the process of tissue regeneration [40]. Dressing remains in direct contact with the wound so the choice of material becomes important. An ideal wound dressing should: 1) provide moist environment, 2) protect against bacterial infection, 3) allow gas exchange between wounded tissue and surrounding environment, 4) enhance epidermal migration, 5) absorb excess exudates without leakage to the

surface of a dressing, 6) increase cell-proliferation, 7) provide thermal insulation to improve the blood flow, 8) promote angiogenesis and tissue synthesis, 9) provide debridement action and protect the wound bed from mechanical trauma, 10) non-adherent to the wound and easy to remove after healing without irritation, and 11) biocompatible, non-toxic, sterile, non-allergic and non-scaring [13,34,41].

#### 3.2.5.1 Types of wound dressing

Currently, based on their function, available wound dressings are divided into three main categories: passive, interactive, and bioactive wound dressings (Tables 3.2 and 3.3).

An ideal wound dressing should be able to enhance the healing process. Nanofibrous scaffold are also used for dressing as it provides high surface-to-volume ratio, high micro-porosity, flexibility and versatility of choosing wide range of potential biopolymers, simulate the architecture of the natural ECM to promote cell adhesion, migration, and proliferation. Natural polymers are known for high biocompatibility, biodegradability and biological characteristics which make them the best candidates for wound dressings [40]. Table 3.3 list some of the commercialized moisture retentive wound dressings with their advantages

**Table 3.2:** Function-based classification of available wound dressing products [40,42,43].

| Category | Product physical shape | Type of wound | Advantages | Limitations |
|---|---|---|---|---|
| Passive | Gauze, sponges, tulle, lint, adsorbent pads, cotton, wool, natural or synthetic bandages, films | Superficial acute wounds with little exudates | Cover the wound to rehabilitate its function underneath | 1. No regulatory function<br>2. Cannot control moisture levels in the wound<br>3. Adheres to wound bed causing mechanical trauma when removed |
| Interactive | Semi-permeable films, semipermeable foams, amorphous hydrogels, hydrocolloids, 2D and 3D constructs made out of biopolymers | Flat, shallow wounds with light to moderate exudates and possibly infected, moderately to highly exudating wounds | 1. Highly elastic and flexible<br>2. Transparent and permeable to water vapor and oxygen<br>3. Effective barrier against penetration of bacteria to the wound<br>4. Regulate wound healing by simple physicochemical means control moisture level | 1. Not suitable for dry or necrotic wounds<br>2. May adheres to wound bed |
| Bioactive | Skin grafts or substitutes, drug-loaded dressings, antimicrobial dressings. | Infected wound, burns, chronic wounds | 1. Highly elastic and flexible<br>2. Proper barrier against contamination<br>3. Tunable adsorptiveness.<br>4. Regulate wound healing by means of physiologically active substances.<br>5. Control the moisture balance in the wound | 1. Excessive costs, fabrication techniques<br>2. Complicated optimization of drug release<br>3. May adheres to wound bed |

**Table 3.3:** Main classes of the moisture retentive wound dressings [22,44,45]

| Wound dressing type | Description | Advantages | Limitations | Commercial names (Brand) |
|---|---|---|---|---|
| **Alginates** | Composed of algae and kelp derived polysaccharides; suitable for exudative wounds | Absorptive, induce hemostasis, and applicable for sinuses | Not for dry wounds; regular dressing change required for the highly drainage producing wounds | Algiderm (Bard), Algisite (Smith & Nephew), Algisorb (Calgon-Vestal), Algosteril (Johnson & Johnson Medical), Kaltostat (ConvaTec), Curasorb (The Kendall Co), Sorbsan (Dow Hickam), Tegaderm™ (3 M) and Kalginate (DeRoyal) |
| **Antibacterial wound dressing patches** | AgNP containing antimicrobial barrier dressing | Offers long-lasting and fast-acting antibacterial barrier; Sustained silver release for 3-7 days with pain relief. | Potential recurrence of silver-resistant bacteria, bluegray discoloration of the skin with increased duration of use. | Acticoat® (Smith & Nephew), SilvaSorb® (Medline Industries, Inc.), Aquacel® Ag Extra™/ Aquacel® Ag™ (ConvaTec) |
| **Films** | Elastic thin layers with adhesive; suitable for donor sites for split-thickness skin grafts | Protect the wounds against invasion of bacteria, gas permeable, transparency enable visual check of the wound | Insufficient removal of fluid, and the fluid drainage could be even destructive for the newly formed epithelium | Tegaderm (3 M Healthcare), Polyskin II (Kendall Healthcare), Bioclusive (Johnson & Johnson Medical), Blisterfilm (The Kendall Co), Omniderm (Omikron Scientific Ltd), Proclude (ConvaTec), Carrafilm (Carrington Lab) |
| **Foams** | Bilayer dressings comprising a hydrophobic foam surface coated with a hydrophilic material; | Moisture absorption and retention, blocks drainage leakage and bacterial invasion, and suitable for the wounds | Possibly sticks firmly to the wound area in case of drainage desiccation | Polymem (Ferris Corp), PolyMem Silver™ (Aspen Medical), Allevyn (Smith & Nephew United), Biopatch (Johnson & Johnson Medical), Curafoam (The Kendall Co), Flexzan (Dow Hickam), Hydrasorb |

| | | | | |
|---|---|---|---|---|
| | suitable for the wounds with low and moderate exudate | located over bony areas, inside body cavities | | (Tyco/Kendall Co), Lyofoam (ConvaTec), and Mepilex (Mölnlycke Health Care) |
| **Gauze** | Cotton based Gauze Bandage Rolls | Affordable and easily available. Protective, reduce bacterial invasion. | Frequent replacement, wound bed adherence, high infection, not for wet wound healing. Removal may damage the new tissue. Need to be combined with other types of dressings. | Softlaps (DattMediproducts), Johnson & Johnson Band-Aid Gauze Pads |
| **Hydrocolloids** | Pliable sheets consisting of water-resistant foams or gels within PU films; suitable for the wounds with poor exudate production | Encourage formation of granulation tissue, are easy to use, and water-resistant | Undergo a gelation process, drainage, and not recommended for cavities | Duoderm(ConvaTec),NuDerm(Johnson&Johnson Medical), Comfeel (ColoplastSween, Inc), Hydrocol (Dow Hickam), Cutinova (Smith & Nephew), Replicare (Smith & Nephew United), and Tegasorb (3 M) |
| **Hydrogels** | Hydrophilic cross-linked polymer networks with high water retention ability; suitable for dry, necrotic wounds | Enable autolytic debridement and confers a comforting effect for the patient | Possible skin maceration regarding highly exudative wounds | Nu-gel (Johnson & Johnson Medical), Tegagel (3 M), FlexiGel (Smith & Nephew), Curagel (The Kendall Co), Clearsite (Conmed Corp), Elasto-Gel (SW Technologies), Hypergel (Scott Health Care), 2nd Skin (Spenco Medical, Ltd), and Transigel (Smith & Nephew) |

Traditional dressings such as bandages, gauzes and cotton wool offer protection against bacteria, but often suffer from the problem of adhesion of the dressing to the wound, causing pain discomfort and scar when removed [41]. This has been the stimulus for the development of new advanced multifunctional biocompatible, bio-absorbable nano-composite wound dressings with anti-scar property.

### 3.2.6 Components of advanced wound dressings

#### 3.2.6.1 Polyvinyl pyrrolidone (PVP)

PVP is bioactive, amphiphilic, non-toxic, temperature-resistant, pH-stable, biodegradable, and biocompatible polymer. Due to its versatile properties, PVP is widely used in the fabrication of wide range of biomedical products such as therapeutics, supporting material in implants, as a bone spacer, in tissue regeneration, wound healing materials, in diagnostics and many more. PVP has been initially used as a plasma substitute during world war II [46]. PVP as a polymer performs diverse functions as an additive, stabilizer, film former, binder in various medical applications and is also FDA approved. However, applications in newer areas such as cosmetics and aeronautics are being explored. It is an ideal choice for the fabrication of nanofibers or nanoscaffolds. With technological advancements like electrospinning, PVP nanofibers have found wide use in biomedical applications like implants (orthopaedic, dental, vaginal, breast), regenerative engineering (neural, cardiac, and pancreatic tissue), ophthalmic, wound healing materials, theranostics and miscellaneous purposes [47].

#### 3.2.6.2 Cerium nitrate

Cerium is a rare earth element of the lanthanide series, which can exist in either $Ce^{+3}$ (fully reduced) or $Ce^{+4}$ (fully oxidized) state. Due to its redox capacity, cerium is an excellent oxygen buffer causing simultaneous oxidation as well as the reduction [48].

The trivalent cerium ($Ce^{3+}$) salts have been used in the biomedical fields due to their bactericidal and anti-oxidant activity [7]. Cerium nitrate has been found effective in the treatment of the severe burn wounds. It helps to reduce immune-suppression in topical cutaneous burns. It has also been used with silver sulfadiazine for effective treatment of ischemic necrotic wounds of lower extremities [49]. Flammacerium is a typical commercial burn cream formulation having cerium nitrate [50]. The ROS-scavenging abilities of Cerium at the wounded site at nanoscale provide an alternative for oxidative-stress and nitrosative-stress. It helps to enhance the level of collagen and hydroxyproline for effective wound healing [8].

### 3.2.6.3 Curcumin as a bioactive agent

Turmeric (*Curcuma longa*) is a popular Indian spice that has been used for centuries in Indian Ayurvedic medicines for the treatment of a variety of diseases such as anorexia, cough, diabetic ulcers, rheumatism and sinusitis. The biologically active constituent curcumin (diferuloyl methane), isolated from the rhizomes of the plant *Curcuma longa* is very rich in phenolics. It is the principal curcuminoid present in turmeric and is responsible for its yellow colour. Curcumin has shown to have significant anti-inflammatory, anti-oxidant, anti-carcinogenic, anti-mutagenic, anti-coagulant and anti-infective effects. Curcumin has also displayed significant wound healing properties. It acts on various stages of the natural wound healing process to hasten healing [19,21,51,52].

#### 3.2.6.3.1 Safety

Animal and human clinical studies have shown that curcumin is extremely safe even at doses as high as 12 g/day [53]. Recent phase-1 clinical trials have shown that curcumin is nontoxic to humans when administered at 8 g/day for up to 3 months.

Curcumin is generally recognized as safe (GRAS) by the United States FDA and has been granted an acceptable daily intake level of 0.1–3 mg/kg body weight by the Joint FAO/WHO Expert Committee on Food Additives, 1996 [54].

#### 3.2.6.3.2 Bioavailability

A major limiting factor of curcumin use for biomedical purposes is its poor water solubility and low oral bioavailability due to rapid systemic elimination [21]. Efforts to circumvent these problems include the development of curcumin nano-formulations using liposomes, polymer nanoparticles, and other synthetic materials. The addition of piperdine, which functions to inhibit the glucronidation of curcumin, has been shown to increase curcumin bioavailability in rats and in human subjects [51,55,56]. The pathway proposed for curcumin absorption, metabolism and fate after oral administration in rodents and humans has been displayed in *Figure* 3.5.

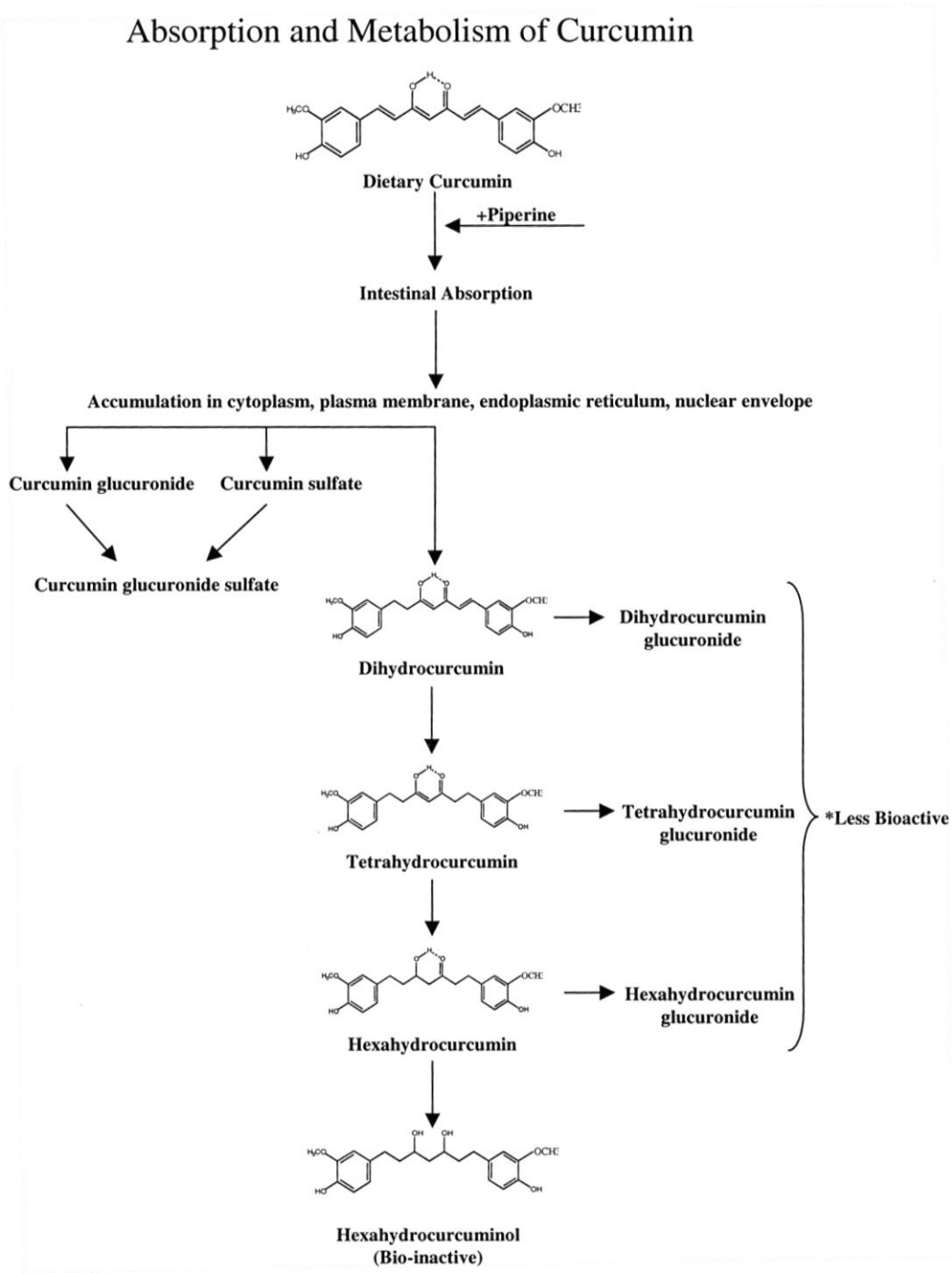


**Figure 3.5:** Absorption, metabolism and fate of curcumin after oral administration in rodents and humans [52].

### 3.2.6.3.3 Application of curcumin

Curcumin has been used to prevent and treat a number of inflammatory diseases. It may be due to its inherent ability to inhibit the inflammatory mediators like cyclooxygenase (cox-2) and lipoxygenase-5 at the transcriptional level [57]. The free radical scavenging activity of curcumin is due to its ability for H-atom donation and resonance stabilization from two phenolic OH groups and from the electron transfer capacity of ß-diketone moiety. In addition, curcumin also regulates the expression of several pro-inflammatory cytokines including tumor necrosis factor (TNF-α), the interleukins (IL-1, IL-2, IL-6, IL-8, IL-12) and some chemokines, most likely through inactivation of the nuclear transcription factor NF-κB [18,58].

### 3.2.6.3.4 Wound healing action mechanisms of curcumin

Curcumin helps in rapid wound healing. Chronic wound is characterized by the persistent inflammation as well as impaired healing process (upper side) however, sustained delivery of curcumin from the topical formulations can effectively modulate various molecular and cellular events (lower side) to accelerate wound healing process as shown in *Figure* 3.6

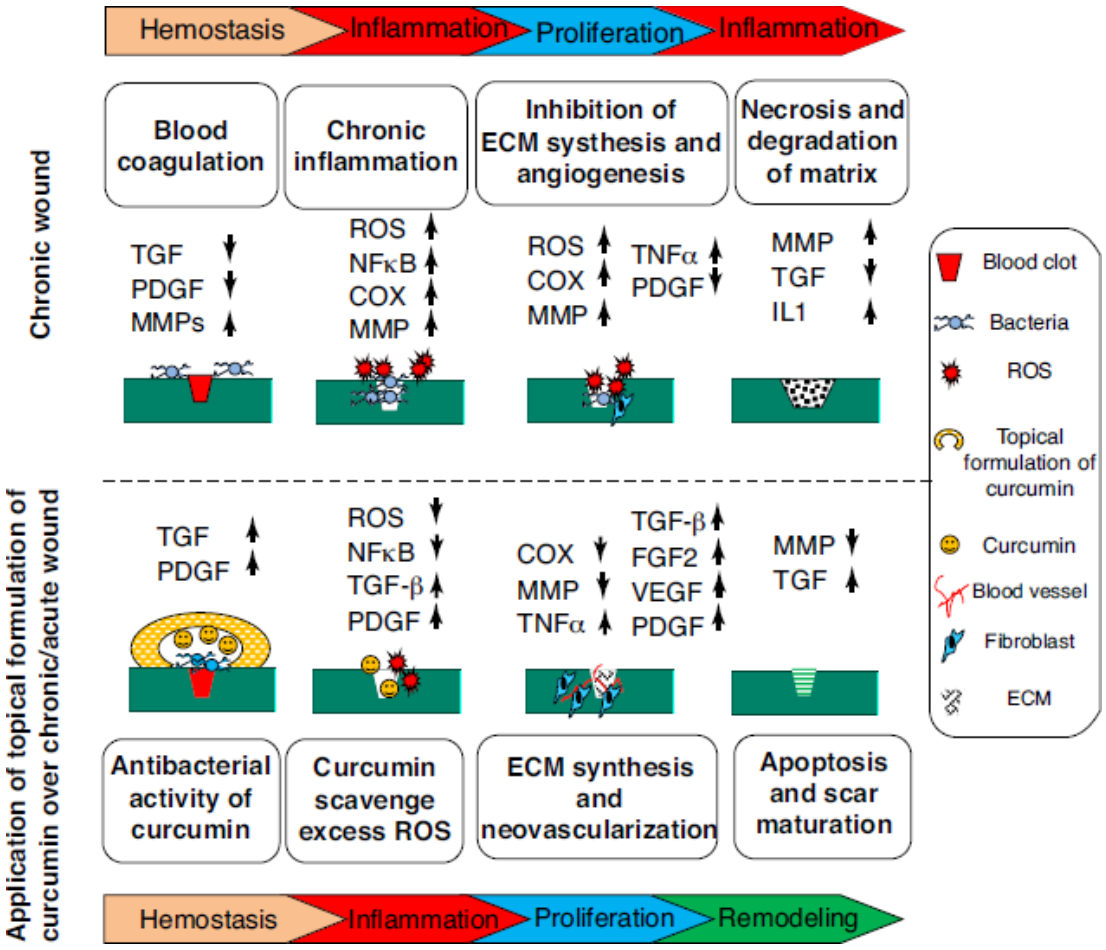


(TGF, transforming growth factors; PDGF, Platelet-derived growth factor; MMPs, Matrix metalloproteinases; NFkB, nuclear factor-kappa B; COX, cyclooxygenase; TNF a, Tumor necrosis factor; IL1, Interleukin-1).

**Figure 3.6:** Effects of topical application of curcumin on different stages of wound healing. [51]

It can be seen that curcumin interferes with the intermediate inflammatory pathways by blocking the nuclear transcription factors. Joe et al. described the mechanisms through which curcumin modulates acute inflammation wound healing process [52]. The details are summarized in Table 3.4.

**Table 3.4:** Action of topical application of curcumin on different stages of wound healing

| Stages of wound healing | Action of curcumin on wound healing process | References |
|---|---|---|
| Inflammation | • Inhibiting the activity of NF-(κ)B transcription factor, reducing the production of TNF-α and IL-1 cytokines, and thereby reducing inflammation<br>• Reduces oxidative stress by reacting with free radicals or ROS and acts as a free-radical scavenger<br>• Inhibits lipid peroxidation and DNA breakage thereby it enhances wound healing activities<br>• Increasing or decreasing the production of anti-oxidant enzymes (dose dependent) | [19,51,58] |
| Proliferation | • Enhancing fibroblast migration, granulation tissue formation, neovascularization, collagen deposition, and in general re-epithelialization<br>• Being apoptotic in the early phase of wound healing, thereby eliminating unwanted inflammatory cells from the wound site to rapidly switch from inflammatory phase to the proliferative phase of healing<br>• It increases the amount of type III collagen relative to type I | [18,51,59] |
| Remodeling | • Improving wound contraction by increasing the production of TGF-β and therefore increasing fibroblast proliferation and wound contraction | [21] |

### 3.2.6.3.5 Recent studies on curcumin application in wound healing

Gadeker et al. formulated curcumin incorporated PVP patches for topical wound-healing application. Studies on an excision rat wound model showed significant wound contraction and rapid wound healing compared to control. Histopathological

results of curcumin patches demonstrated well-ordered collagen fiber and abundant fibroblast cells with new blood vessel formation [60]. Durgaprasad et al. used curcumin cream (BiocurcumaxTM) for topical burn wound healing in Wistar rats. The curcumin-cream-treated group showed significant epithelization and wound contraction compared to the control [61]. Curcumin-loaded emulsion and alginate foams were used in topical formulations and tested in *in vitro* and *in vivo* wound healing studies to ascertain suitability as wound dressing [62,63]. Currently, many commercial anti-oxidant and anti-inflammatory dietary supplements of curcumin are available: BCM-951, TheracurminTM, CurcuVIVATM, CurcuMIND, Longvida RD CAVACURMIN1, BiocurcumaxTM, etc. [51].

## 3.3. Materials and methods

### 3.3.1. Materials

Polyvinyl pyrrolidone (PVP), cerium (III) nitrate hexahydrate ($Ce(NO_3)_3.6H_2O$), 2,2-diphenyl-1-picrylhydrazyl (DPPH), xylazine, eosin Y, disodium salt were procured from Sigma-Aldrich, Saint Louis, Missouri, USA. Ethyl alcohol (99.9%) and methanol were procured from Merck Life Science Pvt. Ltd., Mumbai, Maharashtra, India. Curcumin, dimethyl sulphoxide (DMSO), Dulbecco's modified Eagle medium (DMEM) and supplementary antibiotics, triton® X 100, 3-(4,5-dimethyl-2-thiazolyl)-2,5-diphenyl-2H-tetrazolium bromide (MTT), new born calf serum heat inactivated, buffered formalin fixative, haematoxylin, Luria Bertani (LB) broth, phosphate buffer saline (PBS) and nutrient agar were procured from Himedia Laboratories Pvt. Ltd., Mumbai, Maharashtra, India. 3T6-Swiss albino fibroblast cells were obtained from National Centre for Cell Science (NCCS), Pune, Maharashtra, India. Medical cotton gauze and ciprofloxacin cream (Ciprolar-FC) were purchased from a local medical store

at Varanasi, Uttar Pradesh, India. Double-distilled water (DDW) rinsed and sterilised borosilicate glass-wares were used in various experiments.

### 3.3.2 Preparation of solution for electrospinning of curcumin and cerium loaded nanofibers fabrication

The 10.0% (w/v) PVP solution was prepared in 20 mL ethyl alcohol and 1 mM $Ce(NO_3)_3.6H_2O$ solution in 10 mL of DDW. Both the solutions were stirred continuously for 2 h. 9 mL of the resultant PVP solution was taken in two culture tubes (T1 and T2). In tube T1, 0.09 g of curcumin powder (10% w/w of PVP) was added and stirred for 1 h to form a homogeneous suspension. 3 mL of 1 mM $Ce(NO_3)_3.6H_2O$ aqueous solution was added to tubes T1 and T2 and stirred for 2 h to homogenise. After complete homogenisation, a yellowish solution of PVP-Ce-Cur formed in tube T1 and a transparent solution of PVP-Ce in tube T2. These resultant solutions were electrospun using 5 mL syringes to form fibrous scaffolds of PVP-Ce-Cur NF and PVP-Ce NF, respectively.

Nanofiber preparation by electro-spinning was done using an in-house assembled horizontal electrospinning set up with aluminium foil wrapped flat plate collector. The polymeric electro-spinning solution flow rate through a metallic blunt-end 22 gauges needle was maintained at 2.0 mL/h by a syringe pump. A high DC voltage of 18 kV was applied to generate electrostatic charge driven jet, and the tip-to-collector distance was maintained at 10 cm (*Figure* 3.7, Table 3.5). All the experiments were carried out at the ambient temperature (23 ± 2 °C) and relative humidity of 50-60%. The non-woven nanofibers collected at the grounded flat plate collector were carefully removed and placed in a vacuum desiccator for further use.

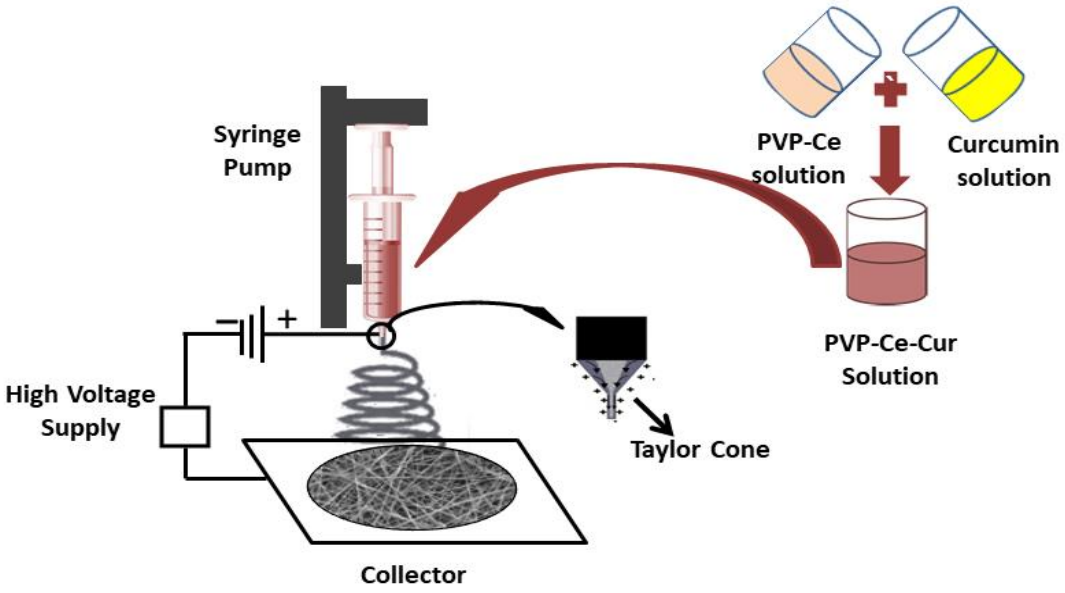


**Figure 3.7:** Schematic diagram of electro-spinning set-up for preparing PVP-based curcumin and ceria loaded electrospun nanofiber

**Table 3.5:** Parameters used for preparing electrospun PVP-based nanofibers

| **Parameters** | **Description** |
|---|---|
| Solvent system for PVP and Curcumin (Cur) | Ethyl alcohol : DDW (3:1 v/v) |
| Co-solvent for cerium (III) nitrate hexahydrate (Ce) | Double distilled water |
| Syringe | A 5 mL syringe fitted with a 22G blunt-end needle |
| Distance between needle and collector | 10 cm |
| Solution Flow rate | 2.0 mL/h |
| Applied DC Voltage | 18 Kv |

### 3.3.3. Physico-chemical characterisation of nanofibers

#### 3.3.3.1 Thickness

A digital micro-meter (Schut Geometrical Metrology, Groningen, Netherlands) was used to measure the thickness of the nanofibers up to the nearest 0.001 mm at five random locations and averaged.

#### 3.3.3.2 Solubility

The solubility of the nanofibers was measured in DDW by immersing a small piece of known dimension (2cm x 2cm) in 50 mL of DDW in a Petri dish. The Petri dish was placed at ambient temperature (23 ± 1 °C) for 6 h. The specimens were dried in the oven at 105 °C for 1h and weighed.

#### 3.3.3.3 Scanning Electron Microscopy (SEM) of Nanofibers

The fiber diameter and surface morphology were examined using ImageJ software and SEM micrograph (FEI, Quanta 200F, Tokyo, Japan) at an acceleration voltage of 20 kV, respectively.

#### 3.3.3.4 Fourier Transforms Infrared (FTIR) Spectroscopy

FT-IR spectroscopic analysis was done to explore the possible chemical interaction between various functional groups of active biomolecules and polymer(s), stability of the biomolecules as well as effect of electro-spinning on the functional groups of constituents in nanocomposites. Spectrum-100 spectrophotometer (Perkin-Elmer, Shelton, USA) was utilized for scanning in the wavelength range of 4200-650 $cm^{-1}$. The FTIR spectra of the samples were obtained directly placing the sample in the sample holder at room temperature (~25 °C).

#### 3.3.3.5 X-ray diffraction (XRD)

In order to evaluate the crystallinity of the nanocomposites, the XRD pattern was recorded in the 2θ range of 10°-60° at a scan rate of 6° $min^{-1}$ using the nickel filtered Cu $K_\alpha$ radiation with a wavelength of 0.154 nm (40 kV, 15 mA) an XRD unit (RigakuMiniflex 600 Desktop X-Ray Diffraction System, RIGAKU Corporation, Tokyo, Japan).

### 3.3.4 Water contact angle (WCA)

The WCA measurements were carried out to evaluate the hydrophilic or hydrophobic nature of the nanofiber surface. The WCA analysis in air was performed by the sessile drop test using a contact angle measuring drop shape analyzer (DSA25S, KRUSS, Hamburg, Germany). A drop of water (4 μL) was dropped on a piece of film (40 mm × 40 mm) placed over the movable stage levelled horizontally using an automatic micro-syringe, and the static images for each surface were taken immediately after dropping the water drop as after 60-90 seconds the water got absorbed in the pores of the scaffold. Five replicate measurements were taken and averaged per nano-fibrous scaffold to represent the mean WCA value of the nanofibers.

### 3.3.5 Nanofiber characteristics

#### 3.3.5.1 *In vitro* free-radical scavenging efficacy of nanofibrous scaffolds

Free-radical scavenging activity measurement for assessing the anti-oxidant capability of the nanofibers was performed by the DPPH assay. It is a colorimetric process for evaluating the anti-oxidant nature of a compound or material. DPPH is a stable radical in solution which develops purple colour in methanol solution with maximum absorbance at 517nm. The principle behind DPPH assay is that DPPH on accepting a hydrogen ion ($H^+$) or an electron from the anti-oxidant gets reduced to

$DPPH_2$, the purple colour changes to yellow with concomitant decrease in absorbance at 517 nm. The change in colour is monitored spectro-photometrically and utilized for the quantification of antioxidant concentration in the solution [64].

5 mg of the nanofibers were immersed separately in 3 mL of DPPH solution in methanol (100µM) and incubated for 0.5 h in the dark at room temperature. After incubation, the reaction mixture was analyzed at $\lambda_{517nm}$ for absorbance using a UV-Visible spectrophotometer (Model 2202, Systronics, Ahmedabad, India). The DPPH scavenging activity was calculated by the equation 3.1:

$$DPPH\ scavenging\ efficacies(\%) = \left(\frac{A_0 - A_n}{A_0}\right) \times 100 \quad (3.1)$$

where, $A_o$ and $A_n$ denote the absorbance at 517 nm of standard DPPH solution and nanofiber immersed DPPH solution, respectively.

**3.3.5.2 In vitro antimicrobial activity**

The antimicrobial activity of the nanofibers was tested against the standard bacterial strains of *Escherichia coli* (ATCC25922) (Gram-negative) and *Staphylococcus aureus* (MTCC1303) (Gram-positive) obtained from the Institute of Medical Sciences, Banaras Hindu University, Varanasi, India. These are commonly found bacteria in open skin wounds. The agar disc diffusion assay was used to analyze the antimicrobial activity of fibrous scaffolds [65]. 100 µL of the overnight grown bacterial cultures ($1\times10^7$ cells/mL) were spread over the nutrient agar plates and incubated for 24 h at 37 ± 1 ºC, after placing the sterile nanofiber pieces. The diameter of the zone of inhibition was measured in millimeters after 24 h.

### 3.3.6 Evaluation of the biocompatibility of the fibrous scaffolds

#### 3.3.6.1 *In vitro* hemocompatibility assessment

Assessment of the hemolytic property of the anti-oxidant loaded nanofibers is essential for preserving the integrity of red blood cells (RBCs) in the newly developed blood vessel. Hemocompatibility was assessed as per the protocol developed by Vijayakumar et al. [66]. 2 mL of human blood was taken and centrifuged at 2300 rpm for 15 min to collect RBCs. The plasma was separated by rinsing thrice with normal saline (0.9%) and discarding the supernatant. Erythrocytes pellets at the bottom were re-suspended in 10 mL of normal saline. A sample of 5 mg of nanofibers were mixed with 2 mL of re-suspended standard RBCs suspension and incubated for 30 min at room temperature. For positive and negative control, an equal volume of standard RBCs suspension was mixed with 1% Triton X-100 (for complete RBC lysis) and normal saline, respectively. After incubation, each sample was centrifuged, and absorbance of supernatant for oxyhemoglobin was recorded at $\lambda_{540nm}$ by UV-Visible spectrophotometer. The percentage of hemolysis was estimated using the equation 3.2:

$$Hemolysis\ (\%) = \left\{\frac{A_{test} - A_{-ve\ control}}{A_{+ve\ control} - A_{-ve\ control}}\right\} \times 100 \qquad (3.2)$$

where, $A_{test}$, $A_{-ve\ control}$ and $A_{+ve\ control}$ denote the absorbance of supernatant with nanofiber, normal saline and triton X-100, respectively.

#### 3.3.6.2 Cytocompatibility assay (MTT assay)

Cytocompatibility of the nanofibers was examined by assessing the viability of the 3T6-Swiss albino fibroblast by the MTT (3-[4,5-dimethylthiazol-2-yl]-2,5-diphenyltetrazolium bromide) assay over nanofibers [67]. The MTT assay is based on

the principle that yellow coloured MTT is reduced by mitochondrial NAD(P)H-dependent oxidoreductase enzymes to an intracellular insoluble purple colour formazan. The cells are then solubilized with an organic solvent and to release the solubilized purple colour formazan reagent, which is measured spectrophotometrically at $\lambda_{570nm}$. Since only metabolically active cells contain (reduced nicotinamide adenine dinucleotide phosphate) NAD(P)H-dependent oxidoreductase enzymes, therefore this assay directly gives the concentration of viable cells.

The fibroblasts cell lines were cultured in DMEM enriched with 10% antibiotics and fetal-calf serum in a humidified $CO_2$ incubator (5% $CO_2$) at 37 ºC. UV sterilized cover-slips attached nanofibers were placed into 96-well microplate. Further, the cultured fibroblast cells ($2\times10^4$ cells/well) detached by trypsin-EDTA (Ethylenediamine tetraacetic acid) were seeded on the fibrous scaffolds and incubated for 24, 48 and 72 h in triplicate. Well without nanofiber was also seeded similarly to act as the positive control. After the incubation period, each micro-plate was further incubated for another 4 h after adding 10 µL MTT (10 mg/mL in PBS) in each well. Afterwards, the MTT solution with culture medium was carefully pipetted out and 200 µL/well DMSO was added to dissolve the internalised formazan crystals in viable cells and form a purple coloured solution proportional to viable cell number. After continuous shaking for 10 min, absorbance at $\lambda_{570nm}$ was recorded with the multimode reader. Cell viability percentage was calculated by the equation 3.3:

$$Cell\ viability\ (\%) = \left\{\frac{A_{test}-A_{DMSO}}{A_{positive\ control}-A_{DMSO}}\right\} \times 100 \qquad (3.3)$$

where, $A_{test}$, $A_{DMSO}$ and $A_{positive\ control}$ denote the optical density of culture medium incubated with a nanofiber, with DMSO and without any nano-fiber, respectively.

### 3.3.7 *In vivo* open-wound healing

The *in vivo* study for open wound healing was carried out after prior approval of all the experimental protocol from the Institutional Animal Ethical Committee of the Banaras Hindu University, Varanasi (No. Dean/2019/IAEC/1231). Twenty healthy Wistar rats of either sex, weighing 200-240 g were divided randomly in four groups of 5 rats each- Group I (gauge treated and used as control), Group II (Ciprofloxacin cream treated for comparative study), Group III (PVP-Ce NF treated to study cerium anti-oxidant effect) and Group IV (PVP-Ce-Cur NF treated to study cumulative cerium and curcumin anti-oxidant and anti-scar effect). The rats of different groups were anesthetized separately by injecting a combination of xylazine (5 mg/kg) and ketamine (35 mg/kg) intra-peritoneally. The dorsal skin surface was shaved and sterilised with ethanol (70% v/v in water). Circular excision wound of full-thickness (~2.5 cm diameter) was made up to the level of subcutaneous panniculus carnosus. Healing wounds were snapped periodically, and the wound area was traced over 2 $mm^2$ graphs using tracing paper. Further progression of healing with time was determined using the equation:

$$Wound\ healing\ progression\ (\%) = \left\{\frac{A_0 - A_t}{A_0}\right\} \times 100 \qquad (3.4)$$

where, $A_0$ and $A_t$ stand for the $0^{th}$ day wound area and the wound area after time t ( i. e. post-wound days 4, 8, 12, 16 and 20), respectively.

On the $8^{th}$ and $16^{th}$ days of post-wound, granulation tissue samples were harvested from the healed area and preserved into three portions for further studies. For histological changes analysis the first portion was preserved in formalin. For

endogenous antioxidant (SOD and catalase) analysis in granulation tissue the second portion of tissues was rinsed with ice-cold saline, homogenized in ice-cold PBS (pH 7.4, 50 mM) and the tissue homogenates were centrifuged for 25 min at 5000 rpm at 5 °C, the supernatants were collected for further analysis [35]. The third portion was acid hydrolyzed for hydroxyproline quantification.

### 3.3.8 Histological examination

#### 3.3.8.1 Histological examination of granulation tissues

In order to study the histological developments, the first portion of the harvested tissues preserved in formalin (10% v/v in neutral buffer) was casted in paraffin, thinly sliced and stained with hematoxylin-eosin (H&E) stains. Histological changes in the stained tissues were observed under the optical microscope.

#### 3.3.8.2 Anti-oxidant enzyme activity in granulation tissues

##### 3.3.8.2.1 Superoxide dismutase (SOD) assay

Superoxide free radical scavenging activity of SOD enzyme was determined in the tissue of previously drawn supernatant as per the modified method described by Ak and Gülçin [58]. Superoxide free radicals ($O_2^{\bullet -}$) were generated in riboflavin/methionine photo-illuminated system prepared in 0.05 M phosphate buffer (pH 7.8) and assayed by the reduction of nitro blue tetrazolium (NBT) to spectrophotometrically detectable colour product (blue formazan) at 560 nm.

For analysis, calculated concentration of riboflavin, methionine and NBT were $1.33\times10^{-5}$, $4.46\times10^{-5}$ and $8.15\times10^{-8}$ M, respectively taken in 3 mL of reaction mixture was illuminated at 25 °C for 40 min to generate ($O_2^{-\bullet}$) which reduced NBT to form blue formazan. It was measured spectrophotometrically at 560 nm. When SOD containing supernatant was added in the above solution, SOD started scavenging the superoxide, thereby inhibiting the reduction of NBT. The reduced absorbance of the reaction

mixture indicates improved superoxide scavenging activity. A reaction mixture devoid of SOD served as control. The activity of SOD was expressed as Unit/mg protein, with the unit being the amount of SOD required to inhibit 50% NBT reduction by superoxide radicals. The possible reactions during SOD assay are shown below:

$$Riboflavin + Methioine \xrightarrow{O_2/fluorescent\ illumination} O_2^{-\cdot}$$

$$Nitro\ blue\ tetrazolium + O_2^{-\cdot} \xrightarrow{reduction} Blue\ formazan\ (abs.560nm)$$

If SOD is present in solution, then it scavenges the $O_2^{-\cdot}$, thereby inhibiting the NBT reduction and hence reduction in formazan concentration:

$$SOD + O_2^{-\cdot} \xrightarrow{reduction} H_2O_2$$

The superoxide radical scavenging activity was calculated by using following equation:

$$Superoxide\ radical\ scavenging\ activity\ (\%) = \left(\frac{A_C - A_S}{A_C}\right) \times 100 \qquad (3.5)$$

where, $A_C$ denotes the absorbance of the reaction mixture without supernatant (control), and $A_S$ is the absorbance of the reaction mixture with supernatant.

The activity of SOD was expressed as Unit/mg protein, i.e. the amount of SOD required to inhibit 50% NBT reduction by superoxide radicals.

**3.3.8.2.2 Catalase assay**

Catalase assay is based on the spectrophotometric measurement of reduction in absorbance of $H_2O_2$ (at 240 nm) due to its decomposition by catalase enzyme into water and molecular oxygen.

$$2H_2O_2 \xrightarrow{catalase} 2H_2O + O_2$$

For analysis, the reaction mixture was prepared by adding 1 mL $H_2O_2$ (30 mM in potassium phosphate buffer, pH 7.4) in 2 mL of supernatants prepared as above. The reaction started immediately after the addition of $H_2O_2$. Diminishing UV-absorbance of the sample was recorded at 240 nm for 3 min at intervals of 30 s. The catalase activity was calculated by the equation 3.6:

$$Catalase\ activity = \left(\frac{2.3}{\Delta t}\right)\left(\frac{a}{b}\right)\left(\log\frac{A_1}{A_2}\right) \quad (3.6)$$

where, $A_1$ and $A_2$ are the absorbance of solution at two consecutive time intervals, a is the dilution factor, b is the protein content (mg/mL), and Δt is the time interval i.e. 0.5 min.

The catalase activity was expressed as Unit/mg protein, with the unit expressed as mM of $H_2O_2$ consumed per min. 10 µL (0.17M) of ethanol was added per mL of supernatants to prevent the formation of inactive complex-II (catalase-$H_2O_2$ complex-II).

### 3.3.8.3 Hydroxyproline content in granulation tissues

About 30% of the total protein of human body accounts for the collagen. Hydroxyproline amino acid is the major constituent of collagen, it accounts for nearly 13-14% of the amino acid content. Thus the quantitative estimation of hydroxyproline serves as an indicator for the collagen biosynthesis. The third portion of the harvested granulation tissues were treated thrice with acetone for 6 h to make samples fat-free then acid hydrolysed (6 N HCl, 50 mg sample/mL) for 6 h at 120 °C for analysis of the hydroxyproline content as a quantitative measure of the collagen deposition and fibrosis as per the protocol developed for acid-hydrolysed granulated tissues by Reddy et al.

[68]. Acid hydrolysis yielded individual amino acids which were then neutralized with 2 N NaOH solution (using phenolphthalein as indicator). 50 µL portion of each hydrolyzate was then added to 96-well plate and mixed with 450 µL of chloramine-T to form pyrrole-2-carboxylate as oxidation product within 25 min of incubation. 500 µL/sample of Ehrlich's solution was added and incubated for 25 min at 65 °C, which resulted in the conversion of pyrrole-2-carboxylate to a chromophore (reddish purple complex) with the absorption maxima at 550 nm. Microplate reader was used to measure the corresponding absorbance of chromophore at 550 nm. Hydroxyproline content was determined from the standard curve of pure hydroxyproline (10-100 µg/mL). The possible reaction mechanism during hydroxyproline assay is shown in *Figure* 3.8.

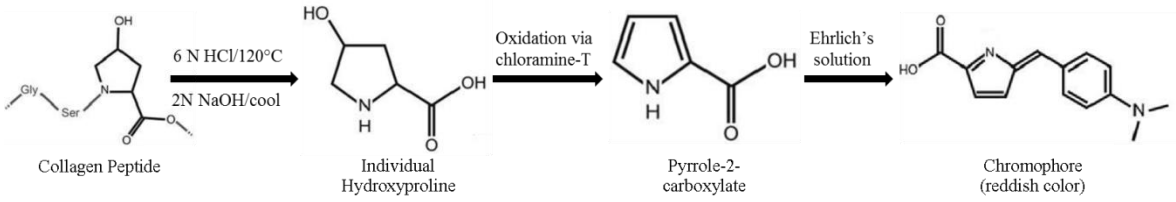


**Figure 3.8:** Reaction mechanism of hydroxyproline assay

### 3.3.8.3.1 Standard curve for hydroxyproline

Serial dilution was used to prepare the standard solutions of hydroxyproline in the concentration range of 10-100 µg/ml from the aqueous working standard solutions (1mg/mL). 450 µL of Chloramine-T was used to oxidize the free hydroxyproline for the production of a pyrrole. 500 µL of Ehrlich's reagent addition resulted in the formation of a reddish-purple colour chromophore which was measured at 550 nm with a microplate

reader and the calibration curve was plotted between concentration and absorbance (*Figure* 3.9).

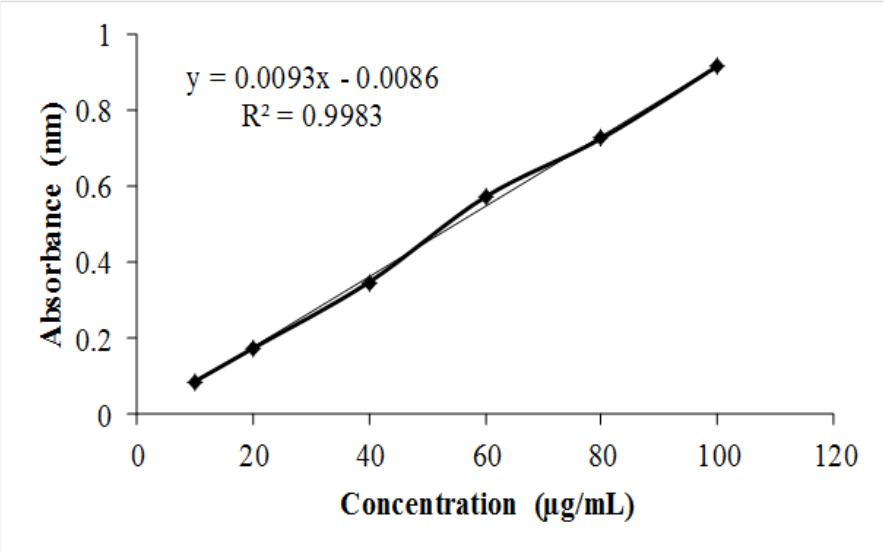


**Figure 3.9:** Calibration curve of hydroxyproline

### 3.3.9 Statistical analysis

All the experiments were carried out at least in triplicate and the results were expressed as mean ± standard deviation. The statistical data comparison was carried out by GraphPad Prizm 5.01 software. The results were either subjected to one-way ANNOVA with Turkey's post-test or two-way ANNOVA with Bonferroni post-test. Results with 95% confidence level ($p < 0.05$) were taken as statistically significant.

## 3.4 Results and discussion

### 3.4.1. Diameter and surface morphology of nanofibers

The SEM images of PVP, PVP-Ce, and PVP-Ce-Cur nanofibers are shown in *Figure* 3.10a through 3.10c and their calculated average diameters are listed in Table 3.6. It is seen that PVP fibers are smooth and have an average diameter of 356.23 ± 119.21 nm**.** The average diameter of PVP-Ce NF and PVP-Ce-Cur NF have ranged from 233.60 ± 139.46 nm and 308.02 ± 106.47 nm, respectively. All fibers have smooth surface and are free from beads. The PVP fibers have the largest diameter. Addition of cerium (III) nitrate hexahydrate has led to reduction in the diameter that can be attributed to the interaction between Cerium ions and PVP chains. However, on addition of curcumin, the diameter has again increased and surface also is less smooth compared to other two fibers (*Figure* 3.10c). The PVP and PVP-Ce nanofibers were of white colour and PVP-Ce-Cur nanofibers were yellowish due to the inherent colour of curcumin.

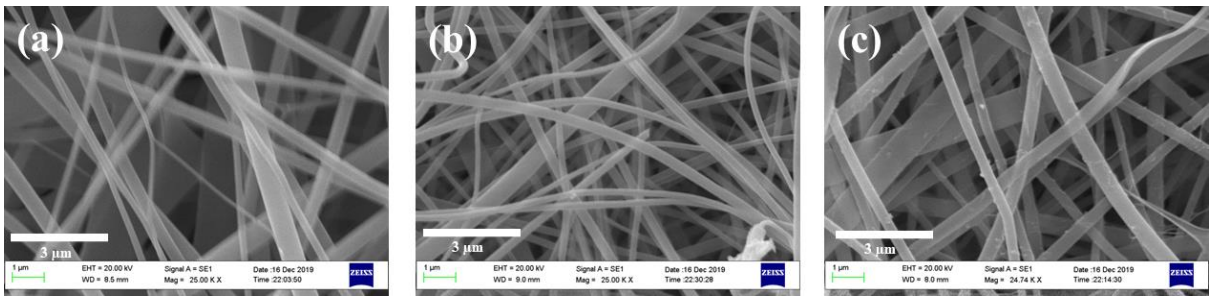


**Figure 3.10:** SEM fingerprints of nanofibers; (a) PVP nanofibers, (b) PVP-Ce nanofibers, (c) PVP-Ce-Cur nanofibers

**Table 3.6:** Morphology, composition, thickness, average fiber diameter and antimicrobial activity of fibrous dressings

| Sr. No. | Nanofibers/ Dressings | Composition | Morphology | Thickness | Diameter of nanofiber | Zone of inhibition for *E. coli* | Zone of inhibition for *S. aureus* |
|---|---|---|---|---|---|---|---|
| | | | | (mm) | (nm) | (mm) | (mm) |
| 1. | PVP NF | A (100%) | Smooth Fibers | 0.019 | 356.23 (±119.21) | 00.0 ± 0.0 | 00.0 ± 0.0 |
| 2. | PVP-Ce NF | A (75%) + B (25%) | Smooth Fibers | 0.016 | 233.60 (±139.46) | 16.0 ± 0.4 | 17.0 ± 0.6 |
| 3. | PVP-Ce-Cur NF | A (75%) + B (25%) + Curcumin | Smooth Fibers | 0.018 | 308.02 ( ±106.47) | 23.0 ± 0.8 | 22.0 ± 0.6 |
| 4. | Gauze | Cotton | Fibrous | 0.038 | - | 00.0 ± 0.0 | 00.0 ± 0.0 |

A- 10% ethanolic polyvinyl pyrrolidone (PVP) solution, B- 1 mM aqueous solution of cerium (III) nitrate hexahydrate, curcumin-10% (w/w of PVP).

### 3.4.2 Physico-chemical characteristics of nanofibers

The PVP and $Ce(NO_3)_3.6H_2O$ both are water-soluble while curcumin is sparingly soluble in water but readily soluble in ethanol. The water uptake and retention capacity of the PVP nanofibers are high and is an ideal wound dressing material [15]. It was observed that PVP and PVP-Ce fibers readily dissolve in water. Curcumin, being less soluble imparts a little hydrophobic characteristic to the fibrous scaffold and thus prolongs dissolution and release. The average thickness of the nanofibers lies in the range of 0.014 - 0.020 mm (Table 3.6).

*Figure* 3.11a shows the FTIR spectra of PVP NF, Curcumin, PVP-Ce NF and PVP-Ce-Cur NF. In the FTIR spectrum of curcumin, the absorption peaks around 3474 to 3616 $cm^{-1}$ show phenolic hydroxyl stretching which may contribute to the formation of hydrogen bonding in PVP-Ce-Cur NF as depicted by a higher intensity of the O–H band. The absorption peaks at 2946 $cm^{-1}$, 1696 $cm^{-1}$, 1510 $cm^{-1}$, 1428 $cm^{-1}$, 1153 $cm^{-1}$ and 960 $cm^{-1}$ correspond to C–H asymmetric stretching vibrations, C=O stretching, aromatic polyphenol skeletal, in-plane aromatic C–C–C or C–C–H deformation, C–O stretching and C–C–H bending, respectively [69]. In the spectrum of PVP NF the absorption peaks at 2926$cm^{-1}$, 2858 $cm^{-1}$, 1694$cm^{-1}$, 860 $cm^{-1}$ can be attributed to the asymmetric $CH_2$ stretching of the pyrrole ring, symmetric C–H stretching, C=O stretching, in-plane $CH_2$ bending respectively [70]. The FTIR spectrum of $Ce(NO_3)_3.6H_2O$ displays the absorption peaks at around 3400 $cm^{-1}$ and 1640 $cm^{-1}$ corresponding to the stretching and bending vibrations of the water molecules, respectively and nitrate ions associated vibrations at about 1450 $cm^{-1}$, 1300 $cm^{-1}$ and 800 $cm^{-1}$[71]. In the FTIR spectrum of PVP-Ce NF, the absorption peaks of phenolic O–H stretching appear at around 3600 $cm^{-1}$, the absorption peaks at 2987 $cm^{-1}$, 1694 $cm^{-1}$

and 1520 $cm^{-1}$ correspond to C–H asymmetric stretching vibrations, C=O stretching and N–H bending, respectively [72]. The spectra of PVP-Ce-Cur NF display higher intensity absorption peaks around 3616 $cm^{-1}$ attributed to phenolic O–H band. A new peak at 3086 $cm^{-1}$ is due to the aromatic C–H stretch. The absorption peaks of curcumin at 1428 $cm^{-1}$, 1153 $cm^{-1}$, 960 $cm^{-1}$ have vanished in the fibrous scaffold possibly due to the intermolecular interactions between the constituents. The FTIR spectra of PVP-Ce-Cur NF and PVP-Ce NF showed typical peaks of the constituents in fingerprint regions with minor variations due to intermolecular interactions, but these interactions did not adversely affect the typical functional groups of the constituents. Thus PVP, $Ce(NO_3)_3.6H_2O$ and curcumin are chemically compatible for the fibrous scaffold. The FTIR spectra show that the curcumin has interacted and altered the PVP chain in PVP-Ce-Cur nano-fibrous scaffold, as supported by the SEM images (*Figure* 3.10) where a change in fiber diameter was observed**.**

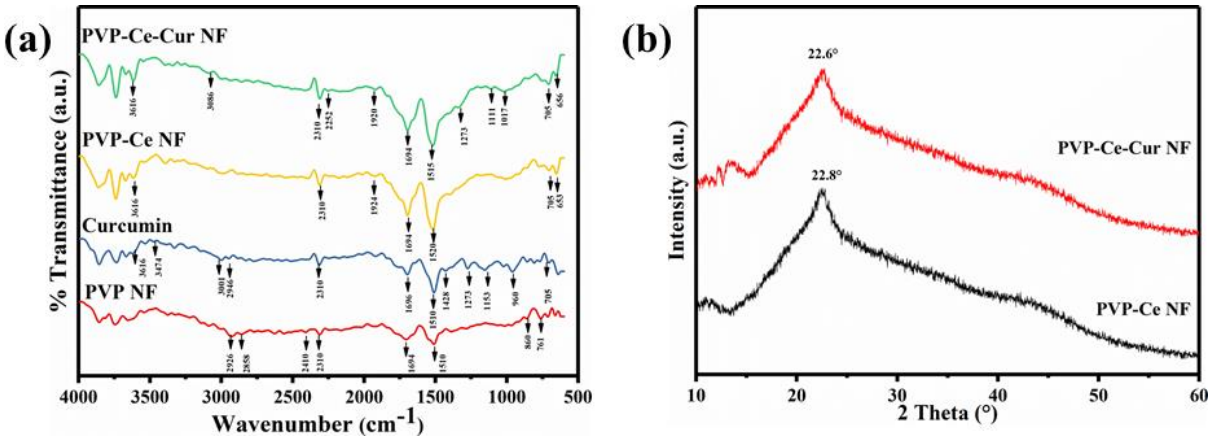


**Figure 3.11:** Fiber characteristics: (a) FTIR spectra of PVP, curcumin, PVP-Ce and PVP-Ce-Cur nano-fibers, (b) XRD patterns of PVP-Ce and PVP-Ce-Cur nanofibers

The X-ray diffraction pattern of the curcumin as discussed by Rahma et al. possess the characteristic intense patterns of a crystalline state at 2θ values of 8.9, 14.54, 17.22, 18.16, and 23.34°. The diffraction pattern of PVP is known to display amorphous form with two broad haloes between 10 and 30° [69]. The presence of PVP in fibrous scaffolds was confirmed by the presence of these two distinct broad haloes in diffractograms of PVP-Ce NF and PVP-Ce-Cur NF (*Figure* 3.11b). It is seen that peaks observed at 2θ of 22.6 and 22.8° are not very sharp and indicate the amorphous nature of both the fibrous scaffolds. Several milder peaks are observed between 2θ of 10 and 15° for PVP-Ce-Cur NF compared to PVP-Ce NF, indicate that the degree of crystallinity of curcumin in PVP-Ce-Cur NF got reduced probably due to aggregation and entrapment of curcumin on the fibers surface (*Figure* 3.10c). Rapid *in-situ* solidification avoided the curcumin recrystallization [73]. This behaviour is supposed to help in the initial burst of curcumin to attenuate ROS. The bioavailability of curcumin got improved in fibrous scaffold due to its amorphous nature.

### 3.4.3 Water contact angle

The sessile water drop contact angle test is used for evaluating the hydrophobic or hydrophilic nature of a surface. The WCA < 90° signifies hydrophilic surfaces while WCA > 90° signifies a hydrophobic surface [74]. It is important to know the behaviour of dressing towards water as the fibroblast adhesion and proliferation on the nanofiber depends on its hydrophilic nature. From *Figure* 3.12, it is seen that pure PVP NF surface is highly hydrophilic and its average WCA is 25.82 ± 2.27°. The WCA for PVP-Ce NF is found to be 54.73 ± 6.27$^{o}$, nearly double that of PVP nanofibers. In case of PVP-Ce-Cur NF it is found to be 78.21 ± 7.24°. Thus it is seen that the hydrophilic nature of fibers has decreased by adding cerium nitrate and curcumin. Based on the

WCA values, the hydrophilicity changes in the order PVP NF > PVP-Ce NF> PVP-Ce-Cur NF.

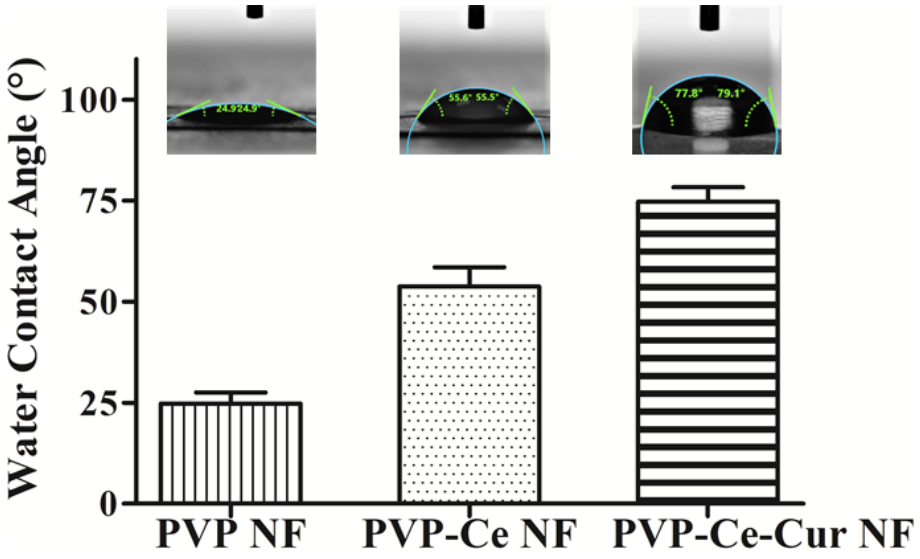


**Figure 3.12:** Water contact angle for PVP NF, PVP-Ce-NF and PVP-Ce-Cur NF. The values are expressed as means ± SD, n=5

### 3.4.4 *In vitro* free-radical scavenging efficacy of nano-fibrous scaffolds

The anti-oxidant activities of the nanofibers were established through DPPH assay (*Figure* 3.13). It is based on the determination of change in the colour of the methanolic DPPH solution. DPPH being a stable free-radical in methanol gives the purple appearance. When any anti-oxidant species comes in its contact and donates an electron or hydrogen ion, the DPPH molecule gets reduced to yellow coloured $DPPH_2$. The change in absorbance value at $\lambda_{517nm}$ is analysed with UV-Visible spectrophotometer to quantify the relative anti-oxidant nature of the formulations [64]. The PVP-Ce NF displayed a scavenging efficiency of 32.76%, which must be due to free-radical scavenging by $Ce^{+3}$[7]**.** The PVP-Ce-Cur NF displayed a scavenging efficiency of 55.13%, probably due to the phenolic groups of curcumin and cerium.

Thus it may be inferred that the anti-oxidant activity got increased due to the synergistic anti-oxidant activity of cerium and curcumin [75]. A significant difference in free-radical scavenging ($p < 0.05$) was observed in nano-fibrous scaffolds with respect to PVP NF due to anti-oxidant activity of cerium and curcumin. PVP-Ce-Cur NF displayed significantly higher ($p < 0.05$) free-radical scavenging compared to PVP-Ce NF due to synergistic anti-oxidant activity.

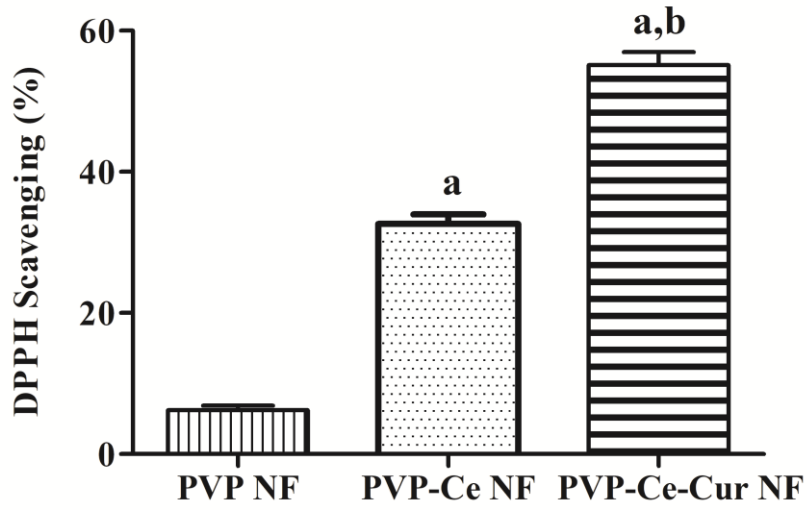


**Figure 3.13:** Free-radical scavenging efficacy of PVP NF, PVP-Ce NF and PVP-Ce-Cur NF obtained through DPPH assay. The values are expressed as means ± SD, n=3, $^{a}p< 0.05$ vs PVP NF, $^{b}p< 0.05$ vs PVP-Ce NF

### 3.4.5 *In vitro* antimicrobial activity

The *in vitro* antimicrobial activity of nanofibers was examined using Gram-positive and gram Gram-negative bacterial species. The PVP NF did not show any antimicrobial activity but a zone of inhibition was observed for PVP-Ce and PVP-Ce-Cur nanofibers. The observed values of the zone of inhibition (Table 3.6) show that

PVP-Ce-Cur NF exhibits maximum antimicrobial activity. The antimicrobial action of the PVP-Ce NF and PVP-Ce-Cur NF is believed to be due to slow release of the active constituents from the nano-fibrous scaffold. The PVP NF did not show any antimicrobial activity. PVP-Ce NF and PVP-Ce-Cur NF both showed antimicrobial activity against *E. coli* and *S. aureus* bacterial species. This behavior could be attributed to the inherent antimicrobial property of cerium and curcumin [7,16,21].

### 3.4.6 Biocompatibility evaluation of the fibrous scaffolds

#### 3.4.6.1 *In vitro* hemocompatibility assesment

The hemocompatibility assessment is essential for scaffold biocompatibility and assessing the integrity, and functionality of the RBCs when exposed to the fibrous scaffolds. Percentage hemolysis value indicates the suitability or non-suitability of fibrous scaffolds. Up to 5% hemolysis by scaffold material is considered suitable [76]. In the present study (*Figure* 3.14a), the PVP NF has shown 3.83% hemolysis, it might be due to high hydrophilicity which results in its dissolution and resultant increase in viscosity. The hemolytic value for PVP-Ce NF was 1.29% and for PVP-Ce-Cur NF was 0.81% which are well within the range of acceptable limits as per the standard norms [66]. A significant difference ($p < 0.05$) was observed with respect to PVP NF due to anti-oxidant activity of cerium and curcumin. Similarly, due to synergistic anti-oxidant activity, PVP-Ce-Cur NF displayed significantly higher ($p < 0.05$) cell viability on the nanofiber surface as compared to PVP-Ce NF. The plausible reason for high cell viability is the protective action of natural curcumin which retards lipid peroxidation and protects thiol group in RBCs membrane from the oxidative damage due to its anti-oxidant property [18].

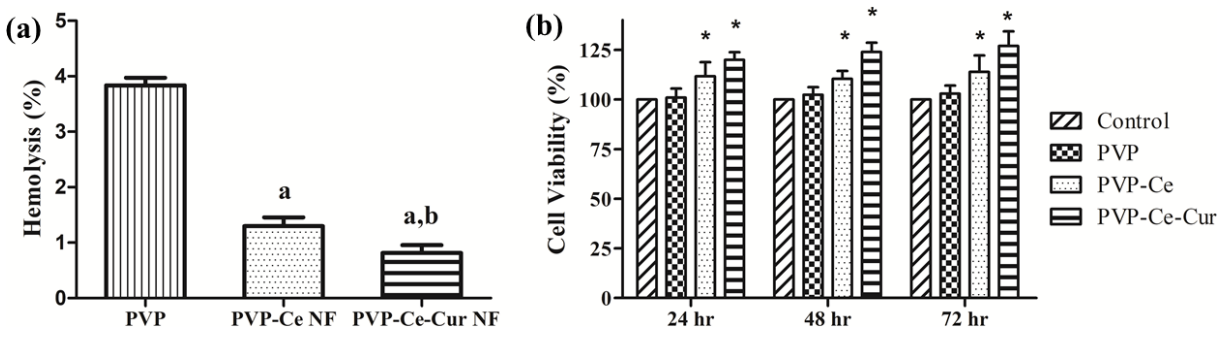


**Figure 3.14:** *In vitro* biocompatibility of fibrous scaffolds: (a) hemocompatibility, (b) cytocompatibility of 3 T6-Swiss albino fibroblast cell lines on different scaffolds after 24 h, 48 h and 72 h incubation. The values are expressed as means ± SD, n=3, $^{a}p< 0.05$ vs PVP NF, $^{b}p< 0.05$ vs PVP-Ce NF, $*p < 0.05$ vs control

### 3.4.6.2 Cytocompatibility assay (MTT assay)

The MTT assay was performed to analyse the viability of 3T6-Swiss albino fibroblast over fibrous scaffolds. The results displayed in *Figure* 3.14b depicted that all the selected fibrous scaffolds were conducive for cell proliferation. The cell lines proliferated well in all the scaffold containing aliquots. All scaffolds showed significantly better ($p < 0.05$) cell viability throughout the study compared to control except PVP NF. The results for PVP-Ce-Cur NF and PVP-Ce NF show that both the fibrous scaffolds are non-toxic and cytocompatible. The increased fibroblast proliferation and collagenesis are due to the curcumin [19].

### 3.4.7 Results of *in vivo* open-wound healing study

The preliminary animal study was conducted to assess the therapeutic potential and efficacy of electrospun nanofibers for effective FTW healing. None of the animals showed post-operative adverse side effects. No case of infection, bleeding of

granulation tissues, sepsis or fluid retention, and death were observed throughout the study. All the four groups of animals remained healthy and by the end of $4^{th}$ week, all members of the groups healed properly. *Figure* 3.15a shows the progressive wound healing on $4^{th}$, $8^{th}$, $16^{th}$ and $20^{th}$ day in the representative Wistar rats of all the four groups (gauze, ciprofloxacin cream, PVP-Ce NF and PVP-Ce-Cur NF treated). The extent of wound healed during the study is shown in *Figure* 3.15b for all the four groups. From *Figure* 3.15a it was inferred that PVP-Ce-Cur NF showed better wound healing at all intervals of time and 100% healing was achieved well before $20^{th}$ days. The most probable reason for accelerated healing might be the reduced microbial infection and ROS level due to the synergistic effect of antimicrobial and anti-oxidant property. The prevention of oxidative damage during inflammatory phase due to cerium in PVP-Ce NF and due to the synergistic effect of cerium and curcumin in PVP-Ce-Cur NF have helped the wounded cells to recover easily from the microbial infection and oxidative shock. From *Figure* 3.15b, it is seen that significant ($p < 0.05$) wound healing/closure has been achieved right from the inflammatory phase to proliferation and maturation phase in PVP-Ce NF and PVP-Ce-Cur NF compared to the control group. In PVP-Ce-Cur NF treated wounds, least scar formation is seen due to the anti-scar property of curcumin. On $16^{th}$ day of the wound healing study, the percentage healing was observed to be 65, 73, 74 and 89% for gauze, ciprofloxacin cream, PVP-Ce NF and PVP-Ce-Cur NF treated wounds, respectively. On the $20^{th}$ day, only PVP-Ce-Cur NF achieved 100% wound healing with least scar, whereas gauze, ciprofloxacin cream and PVP-Ce NF treated groups healed to 79%, 90% and 95%, respectively.

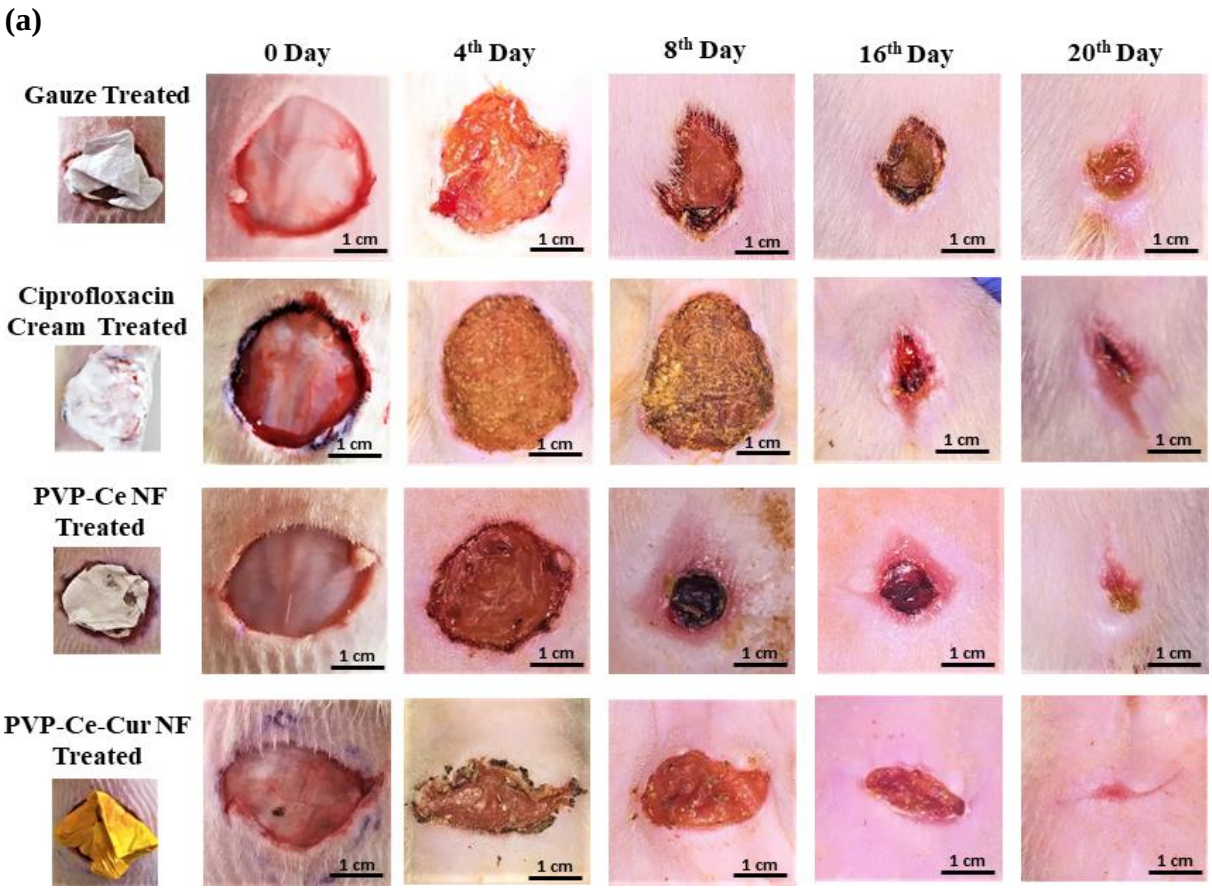


**Figure 3.15:** Effect of dressing materials on healing of full thickness wound: (a) Images of wound healing on day 8 and 16, (b) percentage of wound healed following treatment with gauze, ciprofloxacin cream, PVP-Ce NF and PVP-Ce-Cur NF on day 4, 8, 16 and 20. The values are expressed as means ± SD, n=5,*p < 0.05 vs Gauze treated

### 3.4.8 Histological examinations of granulation tissues

The H&E staining was carried out to visualise the histological changes during tissue granulation. Tissue granulation is the hallmark of wound healing. Gauze, ciprofloxacin cream and fibrous scaffolds treated wounds were evaluated for the granulation tissues on $8^{th}$ and $16^{th}$ day of study. Microscopic images displayed in *Figure* 3.16 show the histological changes in all the four groups on $8^{th}$ and $16^{th}$ day. On $8^{th}$ day, Group-I and Group-II showed high level of infiltrated inflammatory cells and ulceration. In case of Group-III and Group-IV moderate ulceration and inflammatory cells, few proliferating blood vessels of variable shapes and random fibroblast were observed. In the case of PVP-Ce-Cur NF treated wounds (Group-IV), moderate epithelialization with least inflammatory response was observed due to anti-oxidant activity of Cerium and curcumin.

On $16^{th}$ day, incomplete re-epithelialization was observed in Group-I while moderate epithelialization was seen in the Group-II. Partially clear differentiation of dermis and epidermis with a lot of white space in the dermis region, poor collagen, and inflammatory infiltration was seen in both cases. In fibrous scaffold treated groups, Group-III (PVP-Ce NF) and Group-IV (PVP-Ce-Cur NF) a well-developed epidermis with keratinocyte infiltration and dermis layer of skin with good collagen deposition and few inflammatory cells were seen. In Group-III comparatively more inflammatory cells with white spaces corresponding to low collagen deposition were observed in wounds. In Group-IV, it was observed that type-III collagen gets converted to type-I collagen with complete re-epithelialization within 20 days.

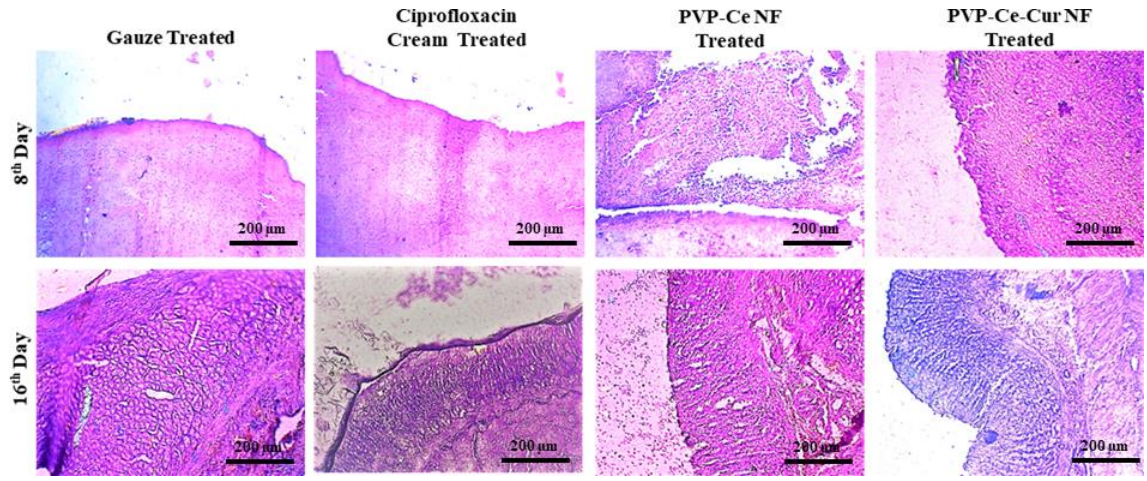


**Figure 3.16:** Histological images (H&E staining) of granulation tissues with gauze, ciprofloxacin cream, PVP-Ce NF and PVP-Ce-Cur NF treatment on day 8 and 16 at 10X microscopic resolution

### 3.4.8.1 Anti-oxidant enzyme activity in granulation tissues

An acute wound exposes the internal cells to microbial infections, and the inflammatory response induces excessive production of ROS as the defence mechanism. The ROS beyond the physiological demand could damage the fibroblast and collagen metabolism and delay the healing process [64]. The endogenous anti-oxidants could not attenuate this oxygen stress in the initial inflammatory phase of 1-4 days. *Figure* 3.17(a-b) showed the anti-oxidant enzyme SOD and catalase activity on $8^{th}$ and $16^{th}$ day of the study. The PVP-Ce NF contains cerium anti-oxidant and PVP-Ce-Cur NF contains dual anti-oxidant in the form of cerium as well as curcumin. These exogenous anti-oxidants in fibrous scaffold could also only partially counter the excess of ROS in the first week as seen from *Figure* 3.17. PVP-Ce-Cur NF showed a significant ($p < 0.05$) improvement in SOD and catalase activity compared to the other groups, and the control. The PVP-Ce NF treated group when compared with gauze and ciprofloxacin

cream treated wound also showed a significant improvement ($p < 0.05$) in enzyme activity due to cerium throughout the study. The ciprofloxacin cream treated wounds showed better activity than the gauze treated, probably due to its antimicrobial activity which attenuated the microbial infections, thus low ROS level. On $16^{th}$ day, PVP-Ce-Cur NF treated group was found to have enhanced SOD and catalase levels compared to the control group ($p > 0.05$) due to dual anti-oxidant activity and low ROS generation during the proliferation phase. Only PVP-Ce-Cur NF treatment was found to effectively attenuate ROS level with endogenous anti-oxidant due to the synergistic antimicrobial and anti-oxidant property of cerium and curcumin.

(a)

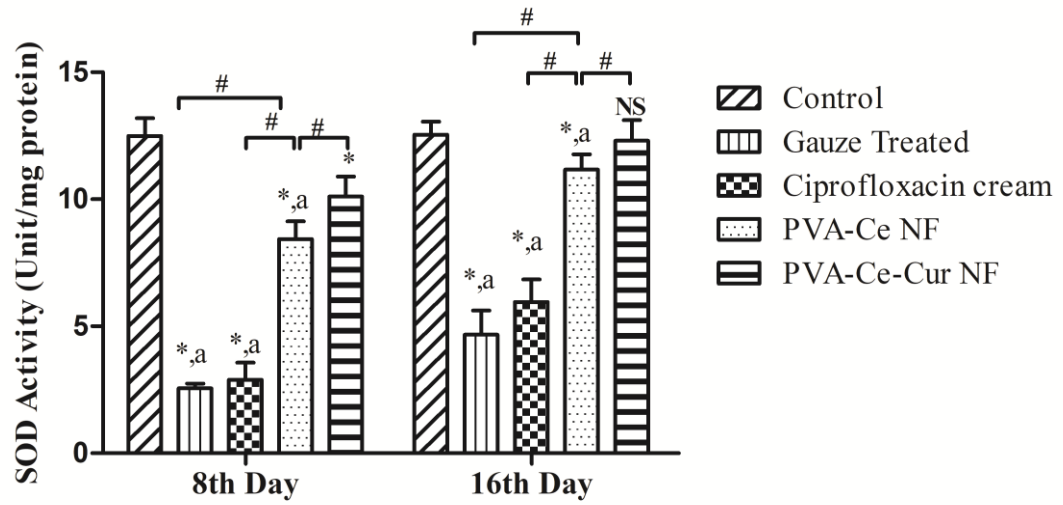


(b)

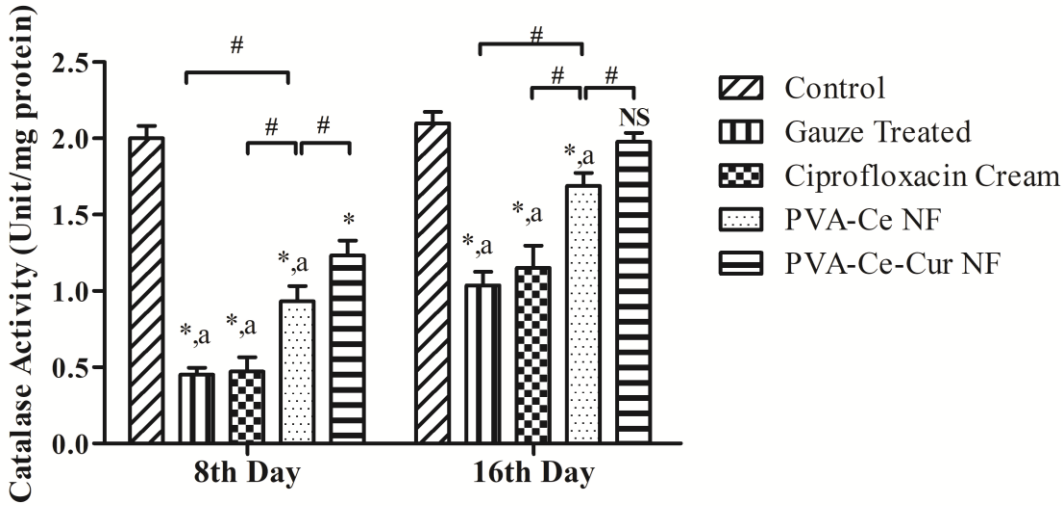


**Figure 3.17:** *In vivo* effect of application of different nanofibers on endogenous enzymes viz. (a) SOD, (b) Catalase in granulation tissues on day 8 and 16. The values are expressed as means ± SD, n=3, *p < 0.05 vs control, $^{a}$p< 0.05 vs PVP-Ce-Cur NF, #p < 0.05 vs PVP-Ce NF treated group, and $^{NS}$p> 0.05 vs control

### 3.4.8.2 Hydroxyproline content in granulation tissues

The hydroxyproline assay is broadly employed as a biochemical index for the collagen fibers formed during the tissue granulation. Higher the content of hydroxyproline or collagen fibre, higher will be the activity of proliferating fibroblast and strengthened regenerated tissues. On $8^{th}$ day, all the fibrous groups showed statistically significant ($p < 0.05$) enhancement in the hydroxyproline level compared to the gauze treated. Ciprofloxacin cream treated wounds were slightly better than gauze treated wounds throughout the study (*Figure* 3.18). On $16^{th}$ day, in the PVP-Ce-Cur NF treated wounds hydroxyproline level peaked to the level of control ($p > 0.05$) and was significantly higher ($p < 0.05$) than all the other groups. The PVP-Ce NF treated wounds showed significant enhancement ($p < 0.05$) in hydroxyproline content compared to gauze and ciprofloxacin cream treated wounds, but not up to the level of PVP-Ce-Cur NF treated wounds. These results depict that dual anti-oxidant loaded PVP-Ce-Cur NF have accelerated the wound healing process by attenuating the oxidative stress of fibroblast, promoting type-I collagen synthesis with accelerated granulation.

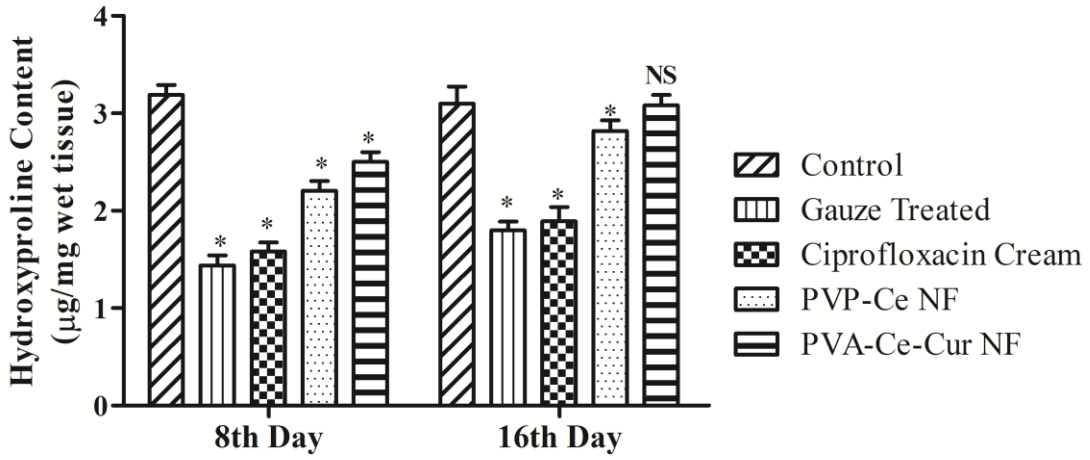


**Figure 3.18:** *In vivo* effect of different dressings on hydroxyproline content in

granulation tissue of Wistar rats on day 8 and 16 of post-wounding. The values are expressed as means ± SD, n=3, *$p < 0.05$ vs control and $^{NS}p > 0.05$ vs control

## 3.5 Conclusion

An electrospun, biomimetic, biocompatible PVP-Ce-Cur nanofibrous scaffold was successfully developed for FTW dressing. It exhibited all the characteristics requirements of a good wound dressing formulation. Its nano-fibrous scaffold prevented microbial infiltration, kept moisture and gaseous exchange at check, and provided high surface area microporous skeletal framework for rapid cell proliferation and granulation. The synergistic anti-oxidant activity of curcumin and cerium helped in the scavenging of ROS, and reduced local oxidative stress *in vivo* for accelerated and anti-scar FTW healing. Curcumin's inherent characteristics helped to reduce the scars with rapid healing. The dissolution of the PVP-Ce-Cur fibrous scaffold with cell maturation will protect the patient from discomfort of wound tissue rupture during removal of dressing.

## References

[1] J. Ding, J. Zhang, J. Li, D. Li, C. Xiao, H. Xiao, H. Yang, X. Zhuang, X. Chen, Electrospun polymer biomaterials, Prog. Polym. Sci. 90 (2019) 1–34.

[2] A. Memic, T. Abudula, H.S. Mohammed, K. Joshi Navare, T. Colombani, S.A. Bencherif, Latest Progress in Electrospun Nanofibers for Wound Healing Applications, ACS Appl. Bio Mater. 2 (2019) 952–969.

[3] E.J. Chong, T.T. Phan, I.J. Lim, Y.Z. Zhang, B.H. Bay, S. Ramakrishna, C.T. Lim, Evaluation of electrospun PCL/gelatin nanofibrous scaffold for wound healing and layered dermal reconstitution, Acta Biomater. 3 (2007) 321–330.

[4] I. Herskovitz, O.B. Hughes, F. Macquhae, A. Rakosi, R. Kirsner, Epidermal skin grafting, Int. Wound J. 13 (2016) 52–56.

[5] G. Ajmal, G.V. Bonde, P. Mittal, G. Khan, V.K. Pandey, B. V. Bakade, B. Mishra, Biomimetic PCL-gelatin based nanofibers loaded with ciprofloxacin hydrochloride and quercetin: A potential antibacterial and anti-oxidant dressing material for accelerated healing of a full thickness wound, Int. J. Pharm. 567 (2019) 118480.

[6] M. Mittal, M.R. Siddiqui, K. Tran, S.P. Reddy, A.B. Malik, Reactive oxygen species in inflammation and tissue injury, Antioxidants Redox Signal. 20 (2014) 1126–1167.

[7] B.C. Nelson, M.E. Johnson, M.L. Walker, K.R. Riley, C.M. Sims, Antioxidant cerium oxide nanoparticles in biology and medicine, Antioxidants. 5 (2016) 1–21.

[8] R. Davan, R.G.S.V. Prasad, V.S. Jakka, R.S.L. Aparna, A.R. Phani, B. Jacob, P.C. Salins, D.B. Raju, Cerium oxide nanoparticles promotes wound healing activity in in-vivo animal model, J. Bionanoscience. 6 (2012) 78–83.

[9] A. Shabunin, V. Yudin, I. Dobrovolskaya, E. Zinovyev, V. Zubov, E. Ivan'kova, P. Morganti, Composite Wound Dressing Based on Chitin/Chitosan Nanofibers: Processing and Biomedical Applications, Cosmetics. 6 (2019) 16.

[10] M. Abrigo, S.L. McArthur, P. Kingshott, Electrospun nanofibers as dressings for chronic wound care: Advances, challenges, and future prospects, Macromol. Biosci. 14 (2014) 772–792.

[11] G.D. Mogoşanu, A.M. Grumezescu, Natural and synthetic polymers for wounds and burns dressing, Int. J. Pharm. 463 (2014) 127–136.

[12] J. Pelipenko, P. Kocbek, J. Kristl, Critical attributes of nanofibers: Preparation, drug loading, and tissue regeneration, Int. J. Pharm. 484 (2015) 57–74.

[13] P. Zahedi, I. Rezaeian, S.O. Ranaei-Siadat, S.H. Jafari, P. Supaphol, A review on wound dressings with an emphasis on electrospun nanofibrous polymeric bandages, Polym. Adv. Technol. 21 (2010) 77–95.

[14] J. Gunn, M. Zhang, Polyblend nanofibers for biomedical applications: Perspectives and challenges, Trends Biotechnol. 28 (2010) 189–197.

[15] M. Teodorescu, M. Bercea, Poly(vinylpyrrolidone) – A Versatile Polymer for Biomedical and Beyond Medical Applications, Polym. - Plast. Technol. Eng. 54 (2015) 923–943.

[16] W.W. Monafo, S.N. Tandon, V.H. Ayvazian, J. Tuchschmidt, A.M. Skinner, F. Deitz, Cerium nitrate: A new topical antiseptic for extensive burns, Surgery. 80 (1976) 465–473.

[17] J.P. Garner, P.S.J. Heppell, Cerium nitrate in the management of burns, Burns. 31 (2005) 539–547.

[18] Y.-H. Yen, C.-M. Pu, C.-W. Liu, Y.-C. Chen, Y.-C. Chen, C.-J. Liang, J.-H. Hsieh, H.-F. Huang, Y.-L. Chen, Curcumin accelerates cutaneous wound healing via multiple biological actions: The involvement of TNF-α, MMP-9, α-SMA, and collagen, Int. Wound J. 15 (2018) 605–617.

[19] D. Akbik, M. Ghadiri, W. Chrzanowski, R. Rohanizadeh, Curcumin as a wound healing agent, Life Sci. 116 (2014) 1–7.

[20] X.Z. Sun, G.R. Williams, X.X. Hou, L.M. Zhu, Electrospun curcumin-loaded fibers with potential biomedical applications, Carbohydr. Polym. 94 (2013) 147–153.

[21] S. Tejada, A. Manayi, M. Daglia, S. F. Nabavi, A. Sureda, Z. Hajheydari, O. Gortzi, H. Pazoki-Toroudi, S. M. Nabavi, Wound Healing Effects of Curcumin: A Short Review, Curr. Pharm. Biotechnol. 17 (2016) 1002–1007.

[22] S. Homaeigohar, A.R. Boccaccini, Antibacterial biohybrid nanofibers for wound dressings, Acta Biomater. 107 (2020) 25–49.

[23] A.D. Juncos Bombin, N.J. Dunne, H.O. McCarthy, Electrospinning of natural polymers for the production of nanofibres for wound healing applications, Mater. Sci. Eng. C. 114 (2020) 110994.

[24] D.J. Tobin, Biochemistry of human skin—our brain on the outside, Chem. Soc. Rev. 35 (2006) 52–67.

[25] M. Takeo, W. Lee, M. Ito, Wound healing and skin regeneration, Cold Spring Harb. Perspect. Med. 5 (2015) a023267.

[26] J. Artem Ataide, L. Caramori Cefali, F. Machado Croisfelt, A. Arruda Martins Shimojo, L. Oliveira-Nascimento, P. Gava Mazzola, Natural actives for wound healing: A review, Phyther. Res. 32 (2018) 1664–1674.

[27] S.A. Eming, B. Brachvogel, T. Odorisio, M. Koch, Regulation of angiogenesis: Wound healing as a model, Prog. Histochem. Cytochem. 42 (2007) 115–170.

[28] L. Cañedo-Dorantes, M. Cañedo-Ayala, Skin acute wound healing: A comprehensive review, Int. J. Inflam. 2019 (2019).

[29] E. Man, C. Hoskins, Towards advanced wound regeneration, Eur. J. Pharm. Sci. 149 (2020) 105360.

[30] D. Simões, S.P. Miguel, M.P. Ribeiro, P. Coutinho, A.G. Mendonça, I.J. Correia, Recent advances on antimicrobial wound dressing: A review, Eur. J. Pharm. Biopharm. 127 (2018) 130–141.

[31] C.I. Günter, H.-G. Machens, New Strategies in Clinical Care of Skin Wound Healing, Eur. Surg. Res. 49 (2012) 16–23.

[32] M. Mahmoudi, L. Gould, Opportunities and Challenges of the Management of Chronic Wounds: A Multidisciplinary Viewpoint, Chronic Wound Care Manag. Res. Volume 7 (2020) 27–36.

[33] S. Chhabra, N. Chhabra, A. Kaur, N. Gupta, Wound Healing Concepts in Clinical Practice of OMFS, J. Maxillofac. Oral Surg. 16 (2017) 403–423.

[34] J. Boateng, O. Catanzano, Advanced Therapeutic Dressings for Effective Wound Healing - A Review, J. Pharm. Sci. 104 (2015) 3653–3680.

[35] R.M. El-Ferjani, M. Ahmad, S.M. Dhiyaaldeen, F.W. Harun, M.Y. Ibrahim, H. Adam, B. Mohd Yamin, M.M.J. Al-Obaidi, R. Al Batran, In vivo Assessment of Antioxidant and Wound Healing Improvement of a New Schiff Base Derived Co (II) Complex in Rats, Sci. Rep. 6 (2016) 1–12.

[36] D. Chouhan, N. Dey, N. Bhardwaj, B.B. Mandal, Emerging and innovative approaches for wound healing and skin regeneration: Current status and advances, Biomaterials. 216 (2019) 119267.

[37] S. Enoch, J.E. Grey, K.G. Harding, Recent advances and emerging treatments, BMJ. 332 (2006) 962–965.

[38] M. Rodrigues, N. Kosaric, C.A. Bonham, G.C. Gurtner, Wound healing: A cellular perspective, Physiol. Rev. 99 (2019) 665–706.

[39] A.C.D.O. Gonzalez, Z.D.A. Andrade, T.F. Costa, A.R.A.P. Medrado, Wound healing - A literature review, An. Bras. Dermatol. 91 (2016) 614–620.

[40] S. Fahimirad, F. Ajalloueian, Naturally-derived electrospun wound dressings for target delivery of bio-active agents, Int. J. Pharm. 566 (2019) 307–328.

[41] S. Dhivya, V.V. Padma, E. Santhini, Wound dressings - A review, BioMedicine. 5 (2015) 24–28.

[42] H.P. Felgueiras, M.T.P. Amorim, Functionalization of electrospun polymeric wound dressings with antimicrobial peptides, Colloids Surfaces B Biointerfaces. 156 (2017) 133–148.

[43] L. Preem, K. Kogermann, Electrospun Antimicrobial Wound Dressings: Novel Strategies to Fight Against Wound Infections, in: Chronic Wounds, Wound Dressings Wound Heal., Springer, Cham, 2018: pp. 213–253.

[44] J.G. Powers, C. Higham, K. Broussard, T.J. Phillips, Wound healing and treating wounds Chronic wound care and management, J. Am. Acad. Dermatol. 74 (2016) 607–625.

[45] H. Choudhury, M. Pandey, Y.Q. Lim, C.Y. Low, C.T. Lee, T.C.L. Marilyn, H.S. Loh, Y.P. Lim, C.F. Lee, S.K. Bhattamishra, P. Kesharwani, B. Gorain, Silver nanoparticles: Advanced and promising technology in diabetic wound therapy, Mater. Sci. Eng. C. 112 (2020) 110925.

[46] H.A. Ravin, A.M. Seligman, J. Fine, Polyvinyl pyrrolidone as a plasma expander; studies on its excretion, distribution and metabolism., N. Engl. J. Med. 247 (1952) 921–929.

[47] M. Kurakula, G.S.N. Koteswara Rao, Moving polyvinyl pyrrolidone electrospun nanofibers and bioprinted scaffolds toward multidisciplinary biomedical applications, Eur. Polym. J. 136 (2020).

[48] M.B. Kolli, The use of cerium oxide and curcumin nanoparticles as therapeutic agents for the treatment of ventricular hypertrophy following pulmonary arterial hypertension, ProQuest Diss. Theses. (2012) 147.

[49] J. Vitse, H. Tchero, S. Meaume, A. Dompmartin, J. Malloizel-Delaunay, C. Géri, C. Faure, C. Herlin, L. Teot, Silver Sulfadiazine and Cerium Nitrate in Ischemic Skin Necrosis of the Leg and Foot: Results of a Prospective Randomized Controlled Study., Int. J. Low. Extrem. Wounds. 17 (2018) 151–160.

[50] J.P. Garner, P.S.J. Heppell, The use of Flammacerium in British Burns Units, Burns. 31 (2005) 379–382.

[51] C. Mohanty, S.K. Sahoo, Curcumin and its topical formulations for wound healing applications, Drug Discov. Today. 22 (2017) 1582–1592.

[52] B. Joe, M. Vijaykumar, B.R. Lokesh, Biological Properties of Curcumin-Cellular and Molecular Mechanisms of Action, Crit. Rev. Food Sci. Nutr. 44 (2004) 97–111.

[53] A. Goel, A.B. Kunnumakkara, B.B. Aggarwal, Curcumin as "Curecumin": From kitchen to clinic, Biochem. Pharmacol. 75 (2008) 787–809.

[54] S.C. Gupta, S. Patchva, B.B. Aggarwal, Therapeutic roles of curcumin: Lessons learned from clinical trials, AAPS J. 15 (2013) 195–218.

[55] G. Shoba, D. Joy, T. Joseph, M. Majeed, R. Rajendran, P.S.S.R. Srinivas, Influence of piperine on the pharmacokinetics of curcumin in animals and human volunteers, Planta Med. 64 (1998) 353–356.

[56] V.K. Pandey, G. Ajmal, S.N. Upadhyay, P.K. Mishra, Nano-fibrous scaffold with curcumin for anti-scar wound healing, Int. J. Pharm. 589 (2020) 119858.

[57] C. V. Rao, Regulation of COX and LOX by curcumin, Adv. Exp. Med. Biol. 595 (2007) 213–226.

[58] T. Ak, I. Gülçin, Antioxidant and radical scavenging properties of curcumin, Chem. Biol. Interact. 174 (2008) 27–37.

[59] B. Fuller, Role of PGE-2 and other inflammatory mediators in skin aging and their inhibition by topical natural anti-inflammatories, Cosmetics. 6 (2019).

[60] R. Gadekar, M.K. Saurabh, G.S. Thakur, A. Saurabh, Study of formulation, characterisation and wound healing potential of transdermal patches of Curcumin, Asian J. Pharm. Clin. Res. 5 (2012) 225–230.

[61] S. Durgaprasad, R. Reetesh, K. Hareesh, R. Rajput, Effect of a topical curcumin preparation ( BIOCURCUMAX ) on burn wound healing in rats Introduction :, J. Pharm. Biomed. Sci. 08 (2011) 1–3.

[62] A.B. Hegge, T. Andersen, J.E. Melvik, E. Bruzell, S. Kristensen, H.H. Tønnesen, Formulation and bacterial phototoxicity of curcumin loaded alginate foams for wound treatment applications: Studies on curcumin and curcuminoides XLII, J. Pharm. Sci. 100 (2011) 174–185.

[63] J.H. Jagannath, M. Radhika, Antimicrobial emulsion (coating) based on biopolymer containing neem (Melia azardichta) and turmeric (Curcuma longa) extract for wound covering, Biomed. Mater. Eng. 16 (2006) 329–336.

[64] K. Mishra, H. Ojha, N.K. Chaudhury, Estimation of antiradical properties of antioxidants using DPPH- assay: A critical review and results, Food Chem. 130 (2012) 1036–1043.

[65] V.K. Pandey, S.N. Upadhyay, K. Niranjan, P.K. Mishra, Antimicrobial biodegradable chitosan-based composite Nano-layers for food packaging, Int. J. Biol. Macromol. 157 (2020) 212–219.

[66] M.R. Vijayakumar, L. Kumari, K.K. Patel, P.R. Vuddanda, K.Y. Vajanthri, S.K. Mahto, S. Singh, Intravenous administration of: Trans -resveratrol-loaded TPGS-coated solid lipid nanoparticles for prolonged systemic circulation, passive brain targeting and improved in vitro cytotoxicity against C6 glioma cell lines, RSC Adv. 6 (2016) 50336–50348.

[67] T.L. Riss, R.A. Moravec, A.L. Niles, S. Duellman, H.A. Benink, T.J. Worzella, L. Minor, Cell Viability Assays, Assay Guid. Man. (2004) 1–25.

[68] G.K. Reddy, C.S. Enwemeka, A simplified method for the analysis of hydroxyproline in biological tissues, Clin. Biochem. 29 (1996) 225–229.

[69] A. Rahma, M.M. Munir, Khairurrijal, A. Prasetyo, V. Suendo, H. Rachmawati, Intermolecular Interactions and the Release Pattern of Electrospun Curcumin-Polyvinyl(pyrrolidone) Fiber, Biol. Pharm. Bull. 39 (2016) 163–173.

[70] A.L. Saroj, R.K. Singh, S. Chandra, Studies on polymer electrolyte poly(vinyl) pyrrolidone (PVP) complexed with ionic liquid: Effect of complexation on thermal stability, conductivity and relaxation behaviour, Mater. Sci. Eng. B Solid-State Mater. Adv. Technol. 178 (2013) 231–238.

[71] M.L. Zheludkevich, J. Tedim, C.S.R. Freire, S.C.M. Fernandes, S. Kallip, A. Lisenkov, A. Gandini, M.G.S. Ferreira, Self-healing protective coatings with "green" chitosan based pre-layer reservoir of corrosion inhibitor, J. Mater. Chem. 21 (2011) 4805–4812.

[72] K.M. Koczkur, S. Mourdikoudis, L. Polavarapu, S.E. Skrabalak, Polyvinylpyrrolidone (PVP) in nanoparticle synthesis, Dalt. Trans. 44 (2015) 17883–17905.

[73] T. Elakkiya, G. Malarvizhi, S. Rajiv, T.S. Natarajan, Curcumin loaded electrospun *Bombyx mori* silk nanofibers for drug delivery, Polym. Int. 63 (2014) 100–105.

[74] V.K. Pandey, K.R. Srivastava, G. Ajmal, V.K. Thakur, V.K. Gupta, S.N. Upadhyay, P.K. Mishra, Differential Susceptibility of Catheter Biomaterials to Biofilm-Associated Infections and Their Remedy by Drug-Encapsulated Eudragit RL100 Nanoparticles, Int. J. Mol. Sci. 20 (2019) 5110.

[75] M.S. Dukhinova, A.Y. Prilepskii, V. V. Vinogradov, A.A. Shtil, Metal oxide nanoparticles in therapeutic regulation of macrophage functions, Nanomaterials. 9 (2019) 1631.

[76] C.J. Chi Perera, M.G. Castillo Baas, G.A. Alcocer Lara, S.I. Ramos Borges, A.L. Rodríguez Guzmán, I. Fernández Cervantes, N. Rodríguez Fuentes, Characterization and hemocompatibility assessment of porous composite scaffolds with a biomimetic human clavicle macrostructure, Health Technol. (Berl). 10 (2019) 423–428.